Front. Phys., 2013, 8(5): 516–539
DOI 10.1007/s11467-013-0382-0

REVIEW ARTICLE

On physics beyond standard model

Yang Hu (胡杨)[1], **You-Kai Wang** (王由凯)[2], **Peng-Fei Yin** (殷鹏飞)[3], **Shou-Hua Zhu** (朱守华)[1,4,†]

[1] *Institute of Theoretical Physics & State Key Laboratory of Nuclear Physics and Technology, Peking University, Beijing 100871, China*

[2] *State Key Laboratory of Theoretical Physics and Kavli Institute for Theoretical Physics China (KITPC), Institute of Theoretical Physics, Chinese Academy of Sciences, Beijing 100190, China*

[3] *Key Laboratory of Particle Astrophysics, Institute of High Energy Physics, Chinese Academy of Sciences, Beijing 100049, China*

[4] *Center for High Energy Physics, Peking University, Beijing 100871, China*

Corresponding author. E-mail: †shzhu@pku.edu.cn

Received July 1, 2013; accepted August 17, 2013

In this review we do not try to cover all the aspects of physics beyond the standard model (BSM), instead *our latest understanding* on the BSM will be presented: i) The Higgs sector is likely related to BSM, which can be confirmed at current running large hadron collider (LHC) or the future colliders. Furthermore we pointed out that spontaneous CP violation can be closely related to the lightness of the Higgs boson. ii) Top quark forward-backward asymmetry, which was measured by Tevatron, might be the sign of BSM. We proposed a new color-octet particle Z_C to account for the observation and Z_C can be further studied at the LHC. iii) If dark matter (DM) is utilized to accommodate astrophysical observations, it ought to be observed at the high energy LHC and DM produced at colliders should be the smoking gun signal. iv) Lithium puzzle might also be the sign of the BSM. We briefly review the newly proposed solution to Lithium puzzle, i.e., the existence of non-thermal component during the big bang nuclei-synthesis (BBN). The possible origins of the non-thermal component can be dark matter or the new accelerating mechanism of normal particles.

Keywords Higgs boson, physics beyond standard model, dark matter, top quark, CP violation

PACS numbers 12.60.i, 12.60.Fr, 14.65.Ha, 13.15.+g, 95.55.Vj, 95.35.+d, 98.62.Gq

Contents

1 Introduction

Since the standard model (SM) formed in the late 1960s and early 1970s, the research on the possible physics beyond the standard model (BSM) is always one of the most active fields [1]. After fifty years, the SM has been confirmed with high precision, which include numerous discoveries and two of them are Higgs boson in 2012 and top quark in 1995. One usually believes that the SM is not the whole story for fundamental physics because it does not contain gravity. Closely related to this issue is that SM does not include the candidate of dark matter (DM), which is required by astrophysical observations.

However there are no confirmed BSM signals until now. The seemingly natural extensions of SM, for example adding the extra gauge bosons and fermions, have been severely constrained. One may wonder where one can discover the BSM. The realistic ways are to precisely measure the properties of Higgs boson and top quark, which are two of the least known particles. Once deviations from the SM predictions are found, we can infer possible BSM information. Moreover the DM is not discovered yet. Normally DM signal can be classified into 3 categories: indirect, direct and collider. Details description on DM signals will be described in Section 4. We should emphasize that the interplay between collider physics and astrophysics is always the driving force to uncover the secretary of Nature.

In this paper, we do not try to cover all aspects of BSM, instead we would like to depict our current understanding on this subject. In Sections 2/3/4/5, Higgs physics, top quark, dark matter and lithium puzzle will be briefly described respectively, and the last section contains discussions and conclusions.

2 Higgs physics

2.1 Higgs sectors as the hiding place for BSM

Recently ATLAS [2] and CMS [3] at Large Hadron Collider have discovered one new particle around 125 GeV with compatible properties with Higgs boson in the SM of high energy physics. However there are still plentiful room for BSM [4]. In fact, the scalar sector is the least known one and relative insensitive to the past measurements. Higgs sectors can be the natural place (in a sense at electro-weak scale) to hide BSM, which could be uncovered at LHC and future high energy/intensity colliders.

Though current measurements on Higgs boson are not so precise, the mass of Higgs boson is approximately fixed without any doubt. Based on the mass information, theoretically there is one question: Why the new particle is so light compared to the possible BSM scale, say O(1 TeV) or higher?

2.2 Why Higgs boson is light?

In the SM, the mass of Higgs boson is a free parameter and could be enormous. The great success of the *renormalizable* SM indicates that there should exist large hierarchy between electro-weak and the higher scale, based on the renormalization group flow analysis of K. Wilson. The Higgs boson, as the spin-0 scalar, tends to get contributions from the higher scale and becomes enormous. Therefore the pursuit of underlying reason why the Higgs boson is light is quite natural. Even before the direct confirmation of the light Higgs boson, one has inferred the similar Higgs boson information from the precision measurements at LEP and Tevatron. Moreover the new ideas have been proposed in order to account for the lightness of the Higgs boson. For example, the lightness of Higgs boson could be protected by supersymmetry. In the minimal supersymmetric model (MSSM), the mass of Higgs boson can be expressed as $m_H < m_Z|\cos(2\beta)|$ at tree level, where m_Z is the Z boson mass and β is the angle defined by $\tan\beta = v_2/v_1$. Here v_2 and v_1 are the vacuum expectation values (VEV) of the two Higgs fields introduced in MSSM. In the little Higgs models, the lightness of Higgs boson is protected by the approximate global symmetry and is treated as the pseudo-Goldstone boson. Though the supersymmtry and little Higgs models are quite intriguing, the experimental search for their companions, namely the gluinos and squarks in supersymmetric models and extra gauge bosons W' and/or Z' in little Higgs models, has failed. Recently we revealed another interesting connection between lightness of Higgs boson and the CP spontaneous violation [5].

CP violation is required in order to account for the matter and anti-matter asymmetry in the Universe, as pointed by Sakharov [6] several decades ago. In the SM, CP non-conservation does exist in the CKM matrix. However such CP violation is not sufficient to accommodate the observed asymmetry [7]. Seeking additional source of CP violation is one of the most important motivations of B-factories, super B-factories and LHCb. In the SM the origin of CP violation in CKM matrix can be traced back to the complex Yukawa interaction among Higgs field and fermions. Besides such explicit CP violation, CP non-conservation can also be traced back to the complex vacuum, as pointed by Lee [8, 9] long time ago. Now that the required additional CP violation and Higgs boson obtain mass via the same mechanism, i.e.,

the spontaneous symmetry breaking, is the Higgs boson mass intimately related to such CP violation? In the following we will show that, taking a simplest spontaneous CP violation model as the example, the mass of the lightest neutral Higgs boson is closely related to CP violation phase of the vacuum. Provided that the SM is not CP-violated, the lightest neutral Higgs boson would be massless, sharing the same characteristic with the neutral Goldstone boson. In reality we require additional CP violation from complex vacuum, as a consequence, the neutral lightest Higgs boson becomes massive and the other neutral Higgs bosons are much heavier than the lightest one. In this sense we relate the lightness of Higgs boson to the complex vacuum. For the most general spontaneous CP violation models, we argue that the lightest neutral Higgs boson can have the exact the same feature as in the simplest case.

2.3 Spontaneous CP violation and lightness of Higgs boson in two Higgs doublets model

One decade ago, we have investigated the simplest spontaneous CP violation model [10, 11] and applied it to the B-meson decay, especially in the large $\tan\beta$ case. The motivations of this model are as following. If one insists the natural flavor conservation (NFC) condition, a minimum of three Higgs doublets are necessary in order to have spontaneous CP violation [12–14]. Provided that NFC is given up, the CP can be explicitly violated in the Higgs potential. However we are only interested in the spontaneous CP violation and investigate its connection with Higgs boson mass. In this paper we will investigate the properties of the Higgs potential for the simplest case of spontaneous CP violation, i.e., only introducing two complex Higgs doublets without obeying NFC condition. In the previous works, we have introduced additional terms which break NFC condition only softly [10, 11].

For two complex Higgs doublets Φ_i $(i = 1, 2)$ with hypercharge $Y = 1$,

$$\Phi_i = \begin{pmatrix} \phi_i^+ \\ \phi_i^0 \end{pmatrix}; \quad \Phi_i^\dagger = \begin{pmatrix} \phi_i^- \\ \phi_i^{0*} \end{pmatrix}$$

ϕ_i^0 and $\phi_i^\pm$ represent neutral and charged complex component of Φ_i, the most general CP-invariant Higgs potential can be written as

$$V(\Phi_1, \Phi_2) = V_2 + V_4$$

It would be better to divide $\Phi_i^\dagger \Phi_j$ term as real and imaginary parts separately: $\mathrm{Re}(\Phi_i^\dagger \Phi_j) \equiv \mathrm{Re}_{ij}$ and $\mathrm{Im}(\Phi_i^\dagger \Phi_j) \equiv \mathrm{Im}_{ij}$ in order to classify the terms conveniently. For $i = j$ imaginary part is 0. Under CP transformation, only imaginary part for $i \neq j$ changes sign. Hermitian and CP invariant require

$$V_2 = m_1^2 \mathrm{Re}_{11} + m_2^2 \mathrm{Re}_{12} + m_3^2 \mathrm{Re}_{22} \tag{1}$$

with m_i^2 $(i = 1 - 3)$ the real parameters.

Hermitian and CP invariant also require

$$\begin{aligned} V_4 = {} & \mathrm{Re}_{11}(\lambda_1 \mathrm{Re}_{11} + \lambda_2 \mathrm{Re}_{12} + \lambda_3 \mathrm{Re}_{22}) \\ & + \mathrm{Re}_{12}(\lambda_4 \mathrm{Re}_{12} + \lambda_5 \mathrm{Re}_{22}) \\ & + \lambda_6 \mathrm{Re}_{22}^2 + \lambda_7 \mathrm{Im}_{12}^2 \end{aligned} \tag{2}$$

where λ_i $(i = 1$–$7)$ are real parameters.

We assume that the minimum of the potential is at

$$\langle \Phi_1 \rangle = \begin{pmatrix} 0 \\ v_1 \end{pmatrix}; \quad \langle \Phi_2 \rangle = \begin{pmatrix} 0 \\ v_2 \mathrm{e}^{\mathrm{i}\xi} \end{pmatrix} \tag{3}$$

which breaks the gauge group $SU(2)_L \otimes U(1)_Y$ down to $U(1)_{em}$ and the CP invariance. We can define $\tan\beta = v_2/v_1, v^2 = v_1^2 + v_2^2$. In the end the v is determined by the mass of weak gauge bosons, as usual.

The requirement of the stationary point of the potential leads to the following constraints:

$$\begin{aligned} \frac{\partial V}{\partial v_1} = {} & 2v_1(m_1^2 + 2\lambda_1 v_1^2 + \lambda_3 v_2^2) \\ & + (m_2^2 + 3\lambda_2 v_1^2 + \lambda_5 v_2^2) v_2 \cos\xi \\ & + 2\lambda_4 v_1 v_2^2 \cos^2\xi + 2\lambda_7 v_1 v_2^2 \sin^2\xi = 0 \end{aligned} \tag{4}$$

$$\begin{aligned} \frac{\partial V}{\partial v_2} = {} & 2v_2(m_3^2 + 2\lambda_6 v_2^2 + \lambda_3 v_1^2) \\ & + (m_2^2 + 3\lambda_5 v_2^2 + \lambda_2 v_1^2) v_1 \cos\xi \\ & + 2\lambda_4 v_1^2 v_2 \cos^2\xi + 2\lambda_7 v_1^2 v_2 \sin^2\xi = 0 \end{aligned} \tag{5}$$

$$\begin{aligned} \frac{\partial V}{\partial \xi} = {} & \sin\xi v_1 v_2 \times (2(\lambda_7 - \lambda_4) v_1 v_2 \\ & \times \cos\xi - m_2^2 - \lambda_2 v_1^2 - \lambda_5 v_2^2) = 0 \end{aligned} \tag{6}$$

For $\sin\xi, v_1, v_2 \neq 0$, we can solve the equations to get

$$m_2^2 = 2(\lambda_7 - \lambda_4) v_1 v_2 \cos\xi - \lambda_2 v_1^2 - \lambda_5 v_2^2 \tag{7}$$

$$m_1^2 = -[2\lambda_1 v_1^2 + (\lambda_3 + \lambda_7) v_2^2 + \lambda_2 v_1 v_2 \cos\xi] \tag{8}$$

$$m_3^2 = -[2\lambda_6 v_2^2 + (\lambda_3 + \lambda_7) v_1^2 + \lambda_5 v_1 v_2 \cos\xi] \tag{9}$$

After substituting those conditions into Higgs potential, we trade v_1, v_2, ξ with m_1^2, m_2^2, m_3^2. It should be emphasized that $\xi = 0$ is the trivial solution of the stationary conditions! In this case Eq. (9) does not necessarily hold [cf. Eq. (6)], the would-be-eliminated parameter by this equation will eventually control the mass of pseudoscalar, usually denoted as A in literature.

The potential minimum conditions require that at the stationary point

$$\frac{\partial^2 V}{\partial v_1 \partial v_1} > 0$$

$$\det\left(\frac{\partial^2 V}{\partial x_i \partial x_j}\right) > 0$$
$$\det\left(\frac{\partial^2 V}{\partial y_i \partial y_j}\right) > 0 \quad (10)$$

where $x_i = v_1, v_2$ and $y_i = v_1, v_2, \xi$.

Now we switch to the spectrum of the physical Higgs bosons. The charged part can be written as $(\phi_1^-, \phi_2^-)M(\phi_1^+, \phi_2^+)$ where the mass matrix

$$M = -\lambda_7 \begin{pmatrix} v_2^2 & -v_1 v_2 e^{-i\xi} \\ -v_1 v_2 e^{i\xi} & v_1^2 \end{pmatrix} \quad (11)$$

The mass eigenstates of G^- and H^- can be written as

$$G^- = e^{i\xi}\sin\beta\phi_2^- + \cos\beta\phi_1^- \quad (12)$$
$$H^- = e^{i\xi}\cos\beta\phi_2^- - \sin\beta\phi_1^- \quad (13)$$

with

$$m_{G^\pm} = 0; \quad m_{H^\pm} = -\lambda_7 v^2 \quad (14)$$

As usual the charged Goldstone boson $G^\pm$ will be absorbed by charged gauge bosons.

For the neutral part, in the basis of $\{\mathrm{Im}(\phi_1), \mathrm{Im}(\phi_2), \mathrm{Re}(\phi_1), \mathrm{Re}(\phi_2)\}$ the symmetric mass matrix M can be expressed as

$$\begin{aligned}
M_{11} &= (\lambda_4 - \lambda_7)v_2^2 \sin^2\xi \\
M_{12} &= \lambda_5 v_2^2 \sin^2\xi \\
M_{13} &= [\lambda_2 v_1 + (\lambda_4 - \lambda_7)v_2\cos\xi]v_2\sin\xi \\
M_{14} &= [(\lambda_4 - \lambda_7)v_1 + \lambda_5 v_2\cos\xi]v_2\sin\xi \\
M_{22} &= 4\lambda_6 v_2^2 \sin^2\xi \\
M_{23} &= [2(\lambda_3 + \lambda_7)v_1 + \lambda_5 v_2\cos\xi]v_2\sin\xi \\
M_{24} &= [\lambda_5 v_1 + 4\lambda_6 v_2\cos\xi]v_2\sin\xi \\
M_{33} &= \frac{1}{2}[8\lambda_1 v_1^2 + 4\lambda_2 v_1 v_2\cos\xi \\
&\quad +(\lambda_4 - \lambda_7)(1+\cos(2\xi))v_2^2] \\
M_{34} &= (2\lambda_3 + \lambda_4 + \lambda_7)v_1 v_2\cos\xi \\
&\quad +\frac{1}{2}[2\lambda_2 v_1^2 + \lambda_5 v_2^2(1+\cos(2\xi))] \\
M_{44} &= (\lambda_4 - \lambda_7)v_1^2 + 2\lambda_5 v_1 v_2\cos\xi \\
&\quad +2\lambda_6 v_2^2(1+\cos(2\xi))
\end{aligned} \quad (15)$$

From mass matrix M, we should note one important feature in the limit of $\xi \to 0$. In this limit, the whole mass matrix can be decomposed into zero and a non-zero $M'_{2\times 2}$ matrices as

$$M = \begin{pmatrix} 0_{2\times 2} & 0_{2\times 2} \\ 0_{2\times 2} & M'_{2\times 2} \end{pmatrix} \quad (16)$$

This feature can be understood because we have applied the constraint of Eq. (9), which is not required for the case of CP conserving $\xi = 0$. One less free parameter drives one of physical neutral Higgs boson massless, sharing the similar feature with neutral Goldstone boson G^0. This point can be shown by rotating away Goldstone state $G^0 = \cos\beta\mathrm{Im}\phi_1^0 + \sin\beta\cos\xi\mathrm{Im}\phi_2^0 - \sin\beta\sin\xi\mathrm{Re}(\phi_2^0)$. We can obtain mass matrix $N_{3\times 3}v^2$ in the basis of

$$\begin{pmatrix} -\sin\beta\mathrm{Im}(\phi_1^0) + \cos\beta\cos\xi\mathrm{Im}(\phi_2^0) - \cos\beta\sin\xi\mathrm{Re}(\phi_2^0) \\ \mathrm{Re}(\phi_1^0) \\ \sin\xi\mathrm{Im}(\phi_2^0) + \cos\xi\mathrm{Re}(\phi_2^0) \end{pmatrix} \quad (17)$$

Here the matrix N can be expressed as

$$\begin{aligned}
N_{11} &= (\lambda_4 - \lambda_7)\sin^2\xi \\
N_{12} &= -[\lambda_2\cos\beta + (\lambda_4 - \lambda_7)\cos\xi\sin\beta]\sin\xi \\
N_{13} &= -[\lambda_5\sin\beta + (\lambda_4 - \lambda_7)\cos\beta\cos\xi]\sin\xi \\
N_{22} &= 4\lambda_1\cos^2\beta + 2\lambda_2\cos\xi\sin\beta\cos\beta \\
&\quad +(\lambda_4 - \lambda_7)\cos^2\xi\sin^2\beta \\
N_{23} &= [2\lambda_3 + 2\lambda_7 + (\lambda_4 - \lambda_7)\cos^2\xi]\sin\beta\cos\beta \\
&\quad \times\lambda_2\cos\xi\cos^2\beta + \lambda_5\cos\xi\sin^2\beta \\
N_{33} &= (\lambda_4 - \lambda_7)\cos^2\beta\cos^2\xi + 2\lambda_5\sin\beta\cos\beta\cos\xi \\
&\quad +4\lambda_6\sin^2\beta
\end{aligned} \quad (18)$$

In the limit of $\xi \to 0$, we can expand the determinant of mass matrix as

$$\begin{aligned}
\det(Nv^2) &= \sin^2(2\beta)\xi^2 v^6[\lambda_7^3 + (2\lambda_3 - \lambda_4)\lambda_7^2 \\
&\quad +(\lambda_3^2 - 2\lambda_3\lambda_4 + \lambda_2\lambda_5 - 4\lambda_1\lambda_6)\lambda_7 - \lambda_1\lambda_5^2 - \lambda_3^2\lambda_4 \\
&\quad +\lambda_2\lambda_3\lambda_5 - \lambda_2^2\lambda_6 + 4\lambda_1\lambda_4\lambda_6] + O(\xi^3)
\end{aligned} \quad (19)$$

The mass of the lightest neutral Higgs boson mass can be written, in the leading order of ξ, as

$$m_{h_1} = f(\lambda_i, \beta)\xi v \quad (20)$$

The mass eigenstate of this neutral Higgs boson approaches $-\sin\beta\mathrm{Im}(\phi_1^0) + \cos\beta\mathrm{Im}(\phi_2^0)$, orthogonal to G^0. Compared with the mass of the SM Higgs boson which is solely determined by λ and VEV, the lightest neutral Higgs boson here is also determined by the CP violation parameter ξ. In the limit of $\xi \to 0$, the lightest neutral Higgs boson and the neutral Goldstone boson both are the mixing states of $\mathrm{Im}(\phi_1^0)$ and $\mathrm{Im}(\phi_2^0)$, sharing the same massless feature. Provided that the SM is not CP-violated, the lightest neutral Higgs boson would be massless. The reality is that the SM is CP-violated[1)], therefore the lightest neutral Higgs boson is massive. In

[1)] Here we refer to the additional CP violation. In fact, the CKM CP violation phase can also be traced back to the complex vacuum.

this sense, the lightness of the lightest Higgs boson is intimately connected to the spontaneous CP violation.

The next question is: Does the mass of the physical lightest neutral Higgs boson in the most general spontaneous CP violation models also approach 0 in the CP invariant limit? The answer is *yes* if the $\xi = 0$ is the trivial solution to equations of the stationary conditions! The arguments are as following. Provided that the original Higgs potential is CP-conserving with certain symmetry. In order to realize the spontaneous symmetry breaking, which gives mass to gauge bosons and induces CP violation, the stationary condition for ξ will eliminate one free parameter in the Higgs potential as in Eq. (6). If $\xi = 0$ is the trivial solution, the would-be-eliminated parameter must be associated with ξ in the mass matrix [c.f. Refs. [15] or [18]]. In the limit of $\xi \to 0$, at least one neutral Higgs boson shares the massless nature of neutral Goldstone boson. Such behavior indicates that the lightness of the Higgs boson can be traced back to the spontaneous CP violation phase of the vacuum.

In the following, we show explicitly the neutral Higgs mass spectrum, especially the lightest one. One can diagonalize the 3×3 real symmetric mass matrix via

$$V_n.\, Nv^2.V_n^{\mathrm{T}} = \frac{1}{2} diag(m_{h_3}^2, m_{h_2}^2, m_{h_1}^2) \tag{21}$$

assuming $m_{h_1} \leqslant m_{h_2} \leqslant m_{h_3}$.

$$\begin{pmatrix} h_3 \\ h_2 \\ h_1 \end{pmatrix} = V_n^{\mathrm{T}} \begin{pmatrix} \cos\beta(\cos\xi \mathrm{Im}(\phi_2^0) - \sin\xi \mathrm{Re}(\phi_2^0)) - \sin\beta \mathrm{Im}(\phi_1^0) \\ \mathrm{Re}(\phi_1^0) \\ \sin\xi \mathrm{Im}(\phi_2^0) + \cos\xi \mathrm{Re}(\phi_2^0) \end{pmatrix} \tag{22}$$

Here matrix V_n can be parameterized by three angles $\theta_i (i = 1 - 3)$ with $0 \leqslant \theta_i \leqslant \pi/2$. The physical quantities can be chosen as $(v, \tan\beta, \xi, m_{h_1}, m_{h_2}, m_{h_3}, \theta_1, \theta_2, \theta_3, m_{H^\pm})$ in accordance with the degree of freedom in Higgs potential. Because the analytical transformation from λ_i to Higgs boson masses and the mixing angles are too lengthy to be useful here, for our purpose, we choose a set of λ_i parameters to illustrate the connection between Higgs boson masses with ξ, especially for m_{h_1}. The benchmark point is chosen as

$$v = 175 \text{ GeV}, \tan\beta = 1, \lambda_7 = -4, \lambda_1 = 4, \lambda_{2,3,4,5,6} = 1$$

This point satisfies the physical requirements. The lightest Higgs boson mass m_{h_1}, m_{h_2} and m_{h_3} are depicted as a function of ξ in Figs. 1–3 respectively. From the figure it is quite clear the dependence of light Higgs approaches massless for the CP conserving case. More importantly, besides the lightest Higgs boson, the other neutral Higgs bosons are much heavier. These three figures clearly demonstrate the crucial role of the spontaneous CP violation parameter ξ.

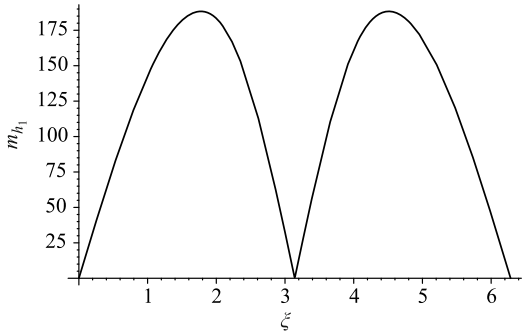

Fig. 1 Lightest Higgs boson mass m_{h_1} [in GeV] as a function of ξ.

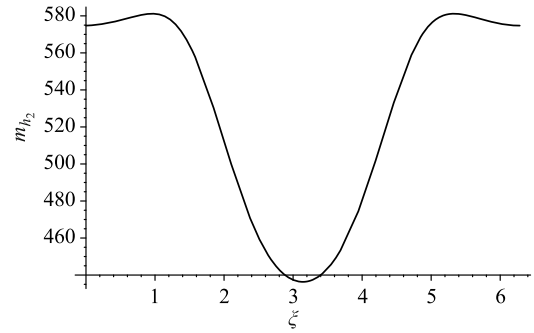

Fig. 2 m_{h_2} [in GeV] as a function of ξ.

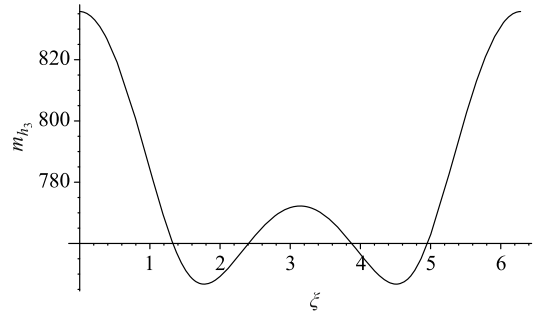

Fig. 3 m_{h_3} [in GeV] as a function of ξ.

2.4 Perspective on Higgs physics

To summarize, we reveal the intimate connection between the spontaneous CP violation and the lightness of the Higgs boson, which was discovered recently by ATLAS and CMS. In the limit of CP conserving case, the lightest Higgs boson degenerates with the massless neutral Goldstone boson. Such connection implies that there should be more Higgs sectors and additional CP violation arising from the complex vacuum. The newly

discovered state with mass around 125 GeV is not a pure CP-even scalar as in the standard model. Instead it is a mixing state of CP-even and CP-odd. Besides the lightest neutral Higgs bosons, there are more much heavier neutral Higgs bosons. We demonstrate this point in the CP-spontaneously broken two-Higgs doublet model and which can be true in the more complicated case. We should emphasize that this is *not* the phenomenological study of the specific model, instead, a toy realization our proposed connection between the complex vacuum and the lightness of the Higgs boson. Further investigations on this direction will be carried out. For the two-Higgs doublet model, current experiments are insensitive to neutral Higgs bosons because the couplings are usually severely suppressed by m_f/m_W for light fermions. It is not hard to find allowed parameters. On the contrary the couplings of top quark with Higgs boson are not suppressed. However the huge QCD backgrounds may bury the signal. Besides the neutral Higgs bosons, there are charged Higgs boson which can be consciously produced at LHC [10, 15, 16].

Last but not least, besides the current running colliders, dedicated Higgs factory may be needed in order to precisely measure the detailed information of the lightest neutral Higgs boson. The whole Higgs spectrum and couplings can only be revealed at the next generation colliders.

3 Top forward-backward asymmetry

3.1 Overview

Being the heaviest particle in the SM, the top quark has some unique properties to make it a good probe to study the new physics. For example, the Yukawa coupling between top quark and the Higgs boson is the most strong among the quarks and Higgs boson and it can significantly change the production and the decay of the Higgs boson; the top quark sometimes is called the bare quark as it decays so fast after its production before the hadronization. Spin information is inherited by its decay products. Except these unique features, the so called the top quark forward–backward asymmetry A_{FB} is considered to be one hint of the new physics.

The top A_{FB} is defined as

$$A_{FB} \equiv \frac{N(\cos\theta > 0) - N(\cos\theta < 0)}{N(\cos\theta > 0) + N(\cos\theta < 0)} \tag{23}$$

in which θ denotes top quark polar angle in a certain frame. Such frame can be taken as the laboratory frame, or usually as the $t\bar{t}$ rest frame. Sometimes it is called the Charge Asymmetry A_C if t and $\bar{t}$ CP conservation is assumed. Experimentally, both the CDF and D0 collaborations have measured the top A_{FB} for several times by utilizing different integrated luminosity data. Excess has been observed compare to the SM predictions. The latest experimental results have been shown in Table 1. It can be seen that the experimental measured result is about 2.2σ larger than the SM NLO predicted value. Such an excess has attracted lots of discussion and is one of the most hot research points about the top quark physics. As the integrated luminosity is increasing, in a recent paper [19], the CDF collaboration has shown the polar angular distribution of the top quark. Such distribution can maintain more information than the half plane integrated forward-backward asymmetry. Discovered at the $p\bar{p}$ collider Tevatron, people are eager to see the cross-check results at the pp collider LHC. Disappointedly, the SM predicted top A_{FB} (usually are called the charge asymmetry A_C at the LHC) is very small (about 0.1%) and the LHC has difficulty to achieve such experimental accuracy in recent measurements [20, 21].

Table 1 The latest top A_{FB} experimental results at the Tevatron [17, 18].

	$\mathcal{L}(fb^{-1})$	A_{FB} (EXP)	A_{FB} (SM NLO)	deviation
CDF	9.4	0.164 ± 0.045	0.066 ± 0.020	2.2σ
D0	5.4	$11.8 \pm 3.2\%$	$4.7 \pm 0.1\%$	2.2σ

In SM, the top A_{FB} origins from the Next-to-Leading Order QCD processes, as shown in Fig. 4. Possible corrections can be contributed from i) interference with the QED process, Eg. A_{FB} can be changed from 0.076 to 0.080 [23]; ii) resummation of the Log terms to all orders. The A_{FB} is stable to this correction, Eg. A_{FB} can be changed from $7.14^{+0.67}_{-0.54}\%$ to $7.16^{+1.05}_{-0.68}\%$ [24]; iii) NNLO QCD process. Although some people have declared the realization of full calculation of the NNLO QCD top pair cross section, the numerical results is still unviable in literature [25]. The A_{FB} is more complicated as it needs the angular distributions rather than the total cross sections.

For explanations beyond the SM, there are quiet a few studies, which includes a flavor changing t-channel Z'/W' [26, 27], the axigluon [28], and many other models. Review of the new model explains can be found in Ref. [29]. However, generally speaking, such explains are all facing very stringent constraints from the experiment point of view. That is they should not only give the correct total A_{FB} numbers, but also should predict the correct differential distributions. Most of the explains are ruled out by the distribution of $\mathrm{d}A_{FB}/\mathrm{d}Y$, $\mathrm{d}A_{FB}/\mathrm{d}M_{t\bar{t}}$, and $\mathrm{d}\sigma/\mathrm{d}M_{t\bar{t}}$, where Y is the rapidity, $M_{t\bar{t}}$ is the top pair invariant mass and σ is the cross section.

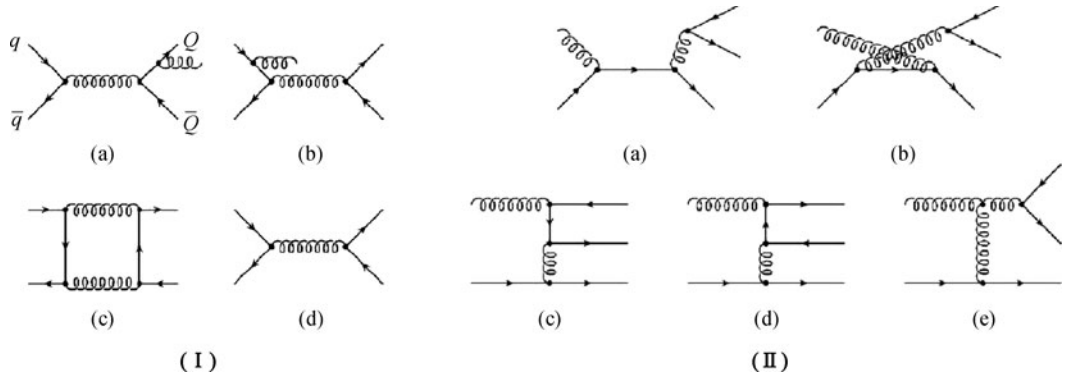

Fig. 4 Origin of A_{FB} at $\mathcal{O}(\alpha_s^3)$ in SM QCD [22]. **(I)** Virtual diagrams, **(II)** Real diagrams.

During recent years, our group have made a series study of the top quark forward–backward asymmetry, which includes: the high order correction of the t-channel Z' model, the new observable A_{OFB} and A_E defined at the LHC, and our proposed explain of the color-octet axial-vector like boson Z_C.

3.2 The high order correction of the t-channel Z'

One of the widely studied explanation of the top A_{FB} excess is the t-channel Z' model, which is proposed in Ref. [26]. By introducing a flavor changing Z' between the up and top quark, asymmetric top distribution can be generated by the interference between the SM $u\bar{u} \to g \to t\bar{t}$ and the t-channel $u\bar{u} \to t\bar{t}$, as shown in Fig. 5. Further more, the contribution of this interference on the symmetric cross section can be canceled with the self-conjugate term by the t-channel $u\bar{u} \to t\bar{t}$ diagram. However, such a t-channel Z' may change the shape of the distribution $\mathrm{d}\sigma/\mathrm{d}M_{t\bar{t}}$. It can be found that such a distribution can not fit the experimental data very well. In the low energy region ($2m_t < M_{t\bar{t}} < 500$ GeV), the predicted cross section values are lower than the experimental measured values; while in the high energy region ($M_{t\bar{t}} > 500$ GeV), the predicted cross section values are larger than the experimental data. We made an analytical calculation of the high order $O(\alpha_s^2\alpha_X)$ correction in the t-channel Z' model [30]. The motivation is to study whether the higher order corrections can improve the fit between t-channel Z' model and the experimental data. The result is shown in Fig. 6. It can be seen that the deviation between t-channel Z' prediction and the experimental data is reduced, but cannot be eliminated. The above mentioned deviation seems to be a generic feature for the t-channel explanation mechanism. Thus we got the conclusion that the t-channel Z' model cannot give a correct $\mathrm{d}\sigma/\mathrm{d}M_{t\bar{t}}$ differential distribution. Besides, such a scenario could also predict the same sign top pair events by the t-channel $uu \to tt$ process, which has already been excluded by the measurement in Ref. [31]. Nevertheless, such a model is in some sense a benchmark model and it is still used by the experimentalists in some recent analysis [19].

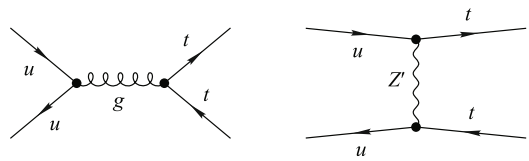

Fig. 5 The interference diagrams between SM and t-channel Z'.

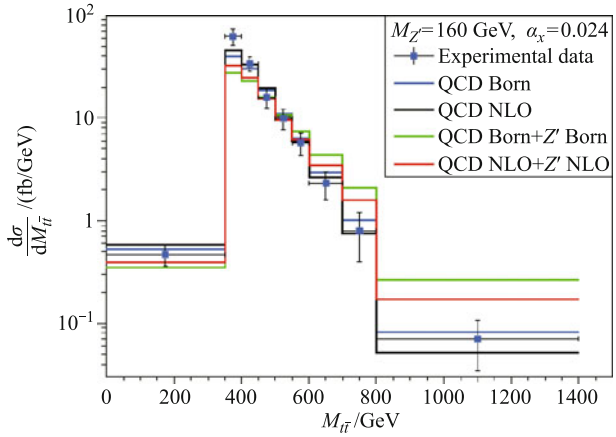

Fig. 6 Differential cross section as a function of $M_{t\bar{t}}$ for different levels [30].

3.3 New observable defined at the LHC

The excess of top A_{FB} was discovered at the $p\bar{p}$ collider Tevatron. To cross check this experiment independently, it is necessary to measure similar observable at the LHC. However, additional problem will occur as the LHC is a pp collider. Opposite to the Tevatron, the symmetric $gg \to t\bar{t}$ component is dominant in the top pair production and it will contribute in the denominator to make the asymmetry very small (at 0.1% level). Thus, it is very necessary to study whether their exists a better observable to exhibit the mechanism of the asymmetric top

productions. We defined two new observable to study the top asymmetry at the LHC.

3.3.1 A_{OFB}

A_{OFB} is defined as

$$A_{OFB} = \frac{F_- + B_-}{F_+ + B_+} \equiv \frac{\sigma^A}{\sigma} \tag{24}$$

with

$$F_\pm = (\sigma(\Delta Y > 0) \pm \sigma(\Delta Y < 0))|_{P^z_{t\bar{t}} > P^z_{cut}, M_{t\bar{t}} > M_{cut}} \tag{25}$$

$$B_\pm = (\sigma(\Delta Y < 0) \pm \sigma(\Delta Y > 0))|_{P^z_{t\bar{t}} < -P^z_{cut}, M_{t\bar{t}} > M_{cut}} \tag{26}$$

where $\Delta Y \equiv Y_t - Y_{\bar{t}}$, $P^z_{t\bar{t}}$ is the top pair's z direction momentum.

We call it the one-side forward-backward asymmetry because after applying the $P^z_{t\bar{t}}$ cut, only one side of the top pair events are survival. The key feature of A_{OFB} is that, at the LHC, usually the momentum of the valence quark is larger than that of the sea quark. If we take the momentum of the u quark as the positive z direction, the events with $P^z_{t\bar{t}} > 0$ will be similar as the Tevatron $p\bar{p}$ case, where the u quark moves to the positive z direction and the $\bar{u}$ quark moves in the opposite z direction. Figure 7 shows the A_{OFB} as a function of P^z_{cut} at the LHC with $\sqrt{s} = 14$ TeV.

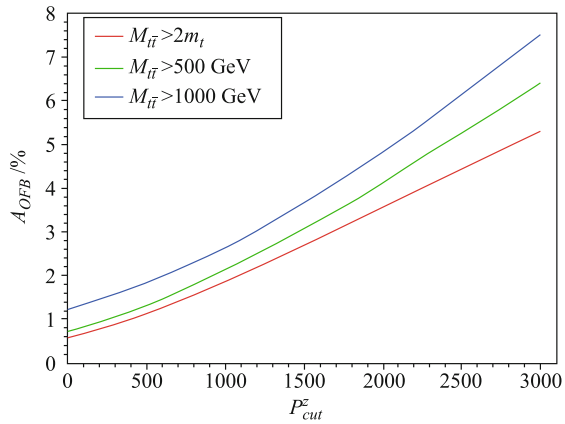

Fig. 7 A_{OFB} as a function of P^z_{cut} at the LHC with $\sqrt{s} = 14$ TeV.

3.3.2 A_E

The above A_{OFB} is defined in the $t\bar{t}$ rest frame. We also studied an asymmetry observable which is defined in the laboratory frame. The edge charge asymmetry is defined as [32]

$$A_E(Y_C, Y_{max}) \equiv \frac{\sigma_t(Y_C < |Y_t| < Y_{max}) - \sigma_{\bar{t}}(Y_C < |Y_{\bar{t}}| < Y_{max})}{\sigma_t(Y_C < |Y_t| < Y_{max}) + \sigma_{\bar{t}}(Y_C < |Y_{\bar{t}}| < Y_{max})} \equiv \frac{\sigma^A_E(Y_C, Y_{max})}{\sigma_E(Y_C, Y_{max})} \tag{27}$$

where Y_C is a critical cut on the rapidity and Y_{max} is the largest rapidity that the detector can cover. A intuitive picture of this definition is that, at the LHC, due to the longitudinal boost of the top quark pair, the top quarks are more likely to be located in the edge region in the detector with large rapidity, and the anti-top quarks are more likely to be located in the central region in the detector with small rapidity. The mechanism of the origin of the asymmetry is the same as shown in Fig. 4 in the SM, and the direction information is also extracted from the feature that in the proton the valence quark's momentum is probably larger than that of the sea quark.

3.4 The color-octet axial-vector like boson

Besides the high order correction in the t-channel Z' model and the definition of new observable at the LHC, we also proposed a new explanation of the excess of the top quark A_{FB}. We introduced a new color-octet axial-vector boson Z_C, where Z indicates that it is a charge neutral particle like the Z boson, and the label C means it carries color octet charge. The mechanism of the additional asymmetry can be explicit by the following squared invariant amplitude:

$$\sum_{\text{Color,Spin}} |\mathcal{M}|^2 = \frac{C_A C_F}{2}\Big\{4g_s^4(1 + c^2 + 4m^2) + \frac{8g_s^2\hat{s}(\hat{s} - M^2_{Z_C})}{(\hat{s} - M^2_{Z_C})^2 + M^2_{Z_C}\Gamma^2_{Z_C}} 2g^q_A g^Q_A c + \frac{4\hat{s}^2}{(\hat{s} - M^2_{Z_C})^2 + M^2_{Z_C}\Gamma^2_{Z_C}}(g^q_A g^Q_A)^2(1 + c^2 - 4m^2)\Big\} \tag{28}$$

where $C_A = 3$, $C_F = 4/3$, g_s is the strong coupling constant, $m = m_t/\sqrt{\hat{s}}$, $\beta = \sqrt{1 - 4m^2}$, $c = \beta\cos\theta$. in which the first term is the contribution from SM gluon mediation; the second term is the interference between $q\bar{q} \to g \to t\bar{t}$ and $q\bar{q} \to Z_C \to t\bar{t}$; the last term is the self-conjugation of the Z_C mediate process. Some characters can be described of the Z_C explanation. i) The additional asymmetry comes from the interference between gluon and Z_C process. This can only change the angular distribution of the produced $t\bar{t}$ events and has no contribution on the total $t\bar{t}$ cross section. ii) The third term of Z_C self-conjugation can contribute to the $t\bar{t}$ total cross section. However, this contribution can be suppressed by

adopting proper coupling factors. iii) The breit-wigner propagator of Z_C shows that Z_C can only impact on its near mass peak region. Actually, our primer idea was to introduce an near top pair production threshold particle to replace the usual heavy (> 1 TeV) axigluon.

The best fitted parameters are $m_{Z_C} = 440$ GeV, $g_A^Q = 3.0$ and $g_A^q = 0.07$ [33]. This is based on the old data which can be replaced by the current more accurate experimental results. In a recent study [34], we update such fit and the best fit diagrams are shown as Fig. 8. Further more, we studied how to cross check this new color-octet axial-vector boson at the LHC. The so-called color flow method is utilized, in which a measurement named the pull is defined as [35]

$$\boldsymbol{t} = \sum_{i\in\text{jet}} \frac{P_T^i |r_i|}{P_T^{\text{jet}}} \boldsymbol{r}_i \tag{29}$$

where $\boldsymbol{r}_i = (\delta y_i, \delta\phi_i) = \boldsymbol{c}_i - \boldsymbol{J}$, and $\boldsymbol{J} = (y_J, \phi_J)$ is the location of the jet and $\boldsymbol{c}_i$ is the position of a cell or particle with transverse momentum P_T^i. Pay attention that $\boldsymbol{t}$ is a two dimensional vector and it can be written as $\boldsymbol{t} = (t_y, t_\phi) = (|\boldsymbol{t}|\cos\theta_t|, |\boldsymbol{t}|\sin\theta_t)$. θ_t is the pole angular determined by the two components of $\boldsymbol{t}$.

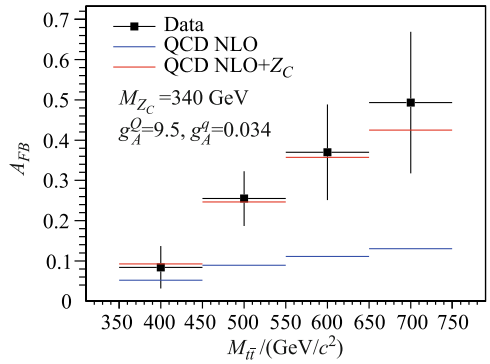

Fig. 8 The differential distributions with best fit Z_C parameters. The experimental data are come from Ref. [17].

Figure 9 shows the comparison of polar angular θ_t of the pull vector at the Tevatron and the LHC. It can be seen that by adopting the new method, our explanation Z_C can be distinguished successfully from the SM at the colliders.

3.5 Perspective on top forward-backward asymmetry

In this paper, we review our studies of the top forward-backward asymmetry excess discovered at the Tevatron. The research includes, i) The high order correction of the t-channel flavor changing Z' explanation. Our studies show that such a model has difficulty to produce correct $\mathrm{d}\sigma/\mathrm{d}M_{t\bar{t}}$ distribution so it is disfavored. ii) We defined

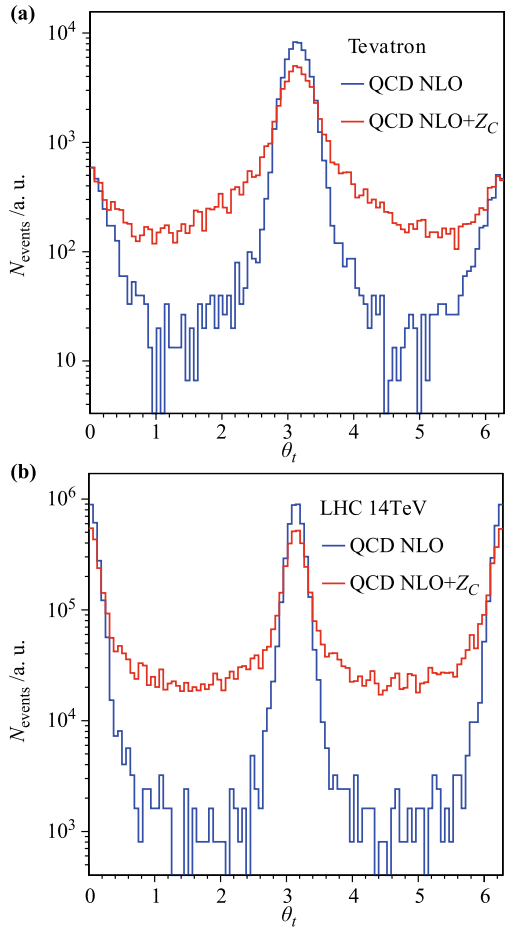

Fig. 9 The distribution of polar angular θ_t of the pull vector $\boldsymbol{t}$ at the Tevatron **(a)** and LHC **(b)**.

two new observable A_{OFB} and A_E which can be measured at the LHC to cross check the top A_{FB} excess. Such observable can be about a few percent level, compare to the usual charge asymmetry at 0.1% level. iii) We proposed a new explain which introduce a color-octet axial-vector like boson Z_C with its mass near the top pair threshold. Such a new particle can produce all experimental differential distributions successfully. We also studied how to measure Z_C's properties at the LHC by the color-flow method.

4 Dark matter

4.1 Evidence for dark matter

The first evidence of DM was proposed by Zwicky in 1930s [36]. The observation of the unexpected large radial velocity dispersion of galaxies in the Coma cluster suggests that it contains more unknown non-luminous matter. Another famous direct evidence of dark matter comes from the observations of spiral galaxy rotation

curves. The rotation velocity of a test object around the center of a galaxy is proportional to $\sqrt{M(r)}/r$ with the orbit radius of r and the mass of $M(r)$ within r. It is expected to decrease quickly as $1/\sqrt{r}$ if the test object is far from the galaxy center. However, the observed rotation curves remain flat at large radii. Such evidences of the non-luminous matter were first found in the Andromeda galaxy in 1930s [37], and were strongly supported by the observations of many galaxies in 1970s [38, 39].

The observations of X-ray emissions from the hot gas in the galaxy clusters show that the gravitation provided by visible matter alone cannot keep the gas in hydrostatic equilibrium. The observations of the lensing effects predicted by general relativity also suggest the existence of non-luminous matter. Since the above results are measured through gravitational effects, some modified Newtonian dynamics (MOND) models were also proposed to interpret these observations and no extra non-luminous matter was needed in such scenarios. An important strong support to the DM hypothesis is the observation on the "Bullet cluster" consisting of two colliding galaxy clusters [40]. The X-ray image, which measures the distribution of the gas, shows an obvious lag compared with the gravitational lensing image. This observation cannot be explained by MOND, but it can be easily understood in the DM scenario, where the DM components can pass through each other without collision, while the gas components have viscous effects.

The standard cosmology model ΛCDM has been established in the last decade from the observations of the cosmic microwave background radiation [41, 42], the distance-redshift relation of the Type Ia supernovae [43, 44] and the large scale structure surveys [45, 46]. Recently, the results from the Planck collaboration show that our Universe consists of 68.3% dark energy, 4.9% baryonic matter and 26.8% DM [42].

4.2 The production and the candidates of dark matter

Although we have so many gravitational evidences for DM from astrophysics and cosmology, we still do not know the particle physics properties of DM. The DM candidates should satisfy the following requirements (see e.g. Ref. [47]):

- They are electrically neutral and colorless particles.
- They are stable in the scale of the Universe lifetime.
- They have the correct relic density $\Omega_{\rm DM}h^2 \sim 0.1$ where $\Omega_{\rm DM} \equiv \rho_{\rm DM}/\rho_0$ is the DM density over the critical density and h is the Hubble constant.
- They are cold or warm (not extremely relativistic) at the structure formation epoch.

In the standard model (SM), neutrinos seem to be the possible DM candidates since they are neutral and interact weakly. However, their relic density calculated by $\Omega_\nu h^2 \sim \sum m_{\nu_i}/(90\ \text{eV}) \sim 0.1$ requires neutrino masses to be ~ 10 eV, which are inconsistent with the experimental limits. Therefore, the SM could not provide a suitable DM candidate. This fact implies the existence of new physics beyond the standard model (BSM).

The most popular DM candidates are the neutral weakly interacting massive particles (WIMPs) (see e.g. Ref. [48]). In such scenarios, DM particles are produced as a thermal relic of the Big Bang [49]. In the early Universe with high temperature, both the SM particles and the WIMPs are in thermal equilibrium $\chi\bar{\chi} \leftrightarrow f\bar{f}$. When the Universe temperature decreases below the WIMP mass, the collisions of the SM particles cannot produce WIMPs efficiently and the number of WIMPs is highly suppressed. If the expanding rate of the Universe is larger than the annihilation rate of the WIMPs, the WIMPs could hardly annihilate with each other and would "freeze out" completely with a constant relic density. This process can be described by the Boltzmann equation

$$\frac{{\rm d}n}{{\rm d}t} = -3Hn - \langle\sigma v\rangle(n^2 - n_{\rm eq}^2) \tag{30}$$

where n is the number density of DM, $n_{\rm eq}$ is the number density in thermal equilibrium, H is the Hubble parameter, and $\langle\sigma v\rangle$ is the thermally averaged annihilation cross section.

The DM relic density can be approximately obtained by

$$\Omega_{\rm DM}h^2 \sim \frac{3\times10^{-27}{\rm cm}^3\cdot{\rm s}^{-1}}{\langle\sigma v\rangle} \tag{31}$$

This means the WIMPs thermally produced with $\langle\sigma v\rangle \sim 3\times10^{-26}{\rm cm}^3\cdot{\rm s}^{-1}$ would have correct DM relic density. In particular, the required value can be easily acquired for the WIMP by $\langle\sigma v\rangle \sim \alpha^2/m^2$ with a mass of $m \sim O(10^2)$ GeV and a interaction coefficient of $\alpha \sim O(10^{-2})$. This feature, often called "WIMP miracle", is an important reason why the WIMPs are the most well-motivated DM candidates. WIMPs as the DM candidates have been proposed in many popular BSM models, such as the lightest supersymmetric particle (LSP) in the supersymmetry (SUSY) model [50] and the lightest Kaluza–Klein particle in the universal extra dimension model [51]. In these models, WIMPs are stable due to some extra discrete symmetries. They have the masses of 100 GeV∼1 TeV and weak interaction with the SM particles, and could be tested at collider experiments. The other possible DM candidates include sterile neutrinos [52, 53], axions [54], etc.

To determine the nature of the DM particles, we should detect the interactions between the DM and SM particles beyond the gravitation. There are three kinds of methods to detect such interactions, namely, direct, indirect and collider detections. The direct detection detects the scattering between the DM and the SM particles via the nuclear recoil signatures in the detector. The indirect detection searches for the energetic cosmic-ray (CR) particles, such as photons, neutrinos and antimatter particles, induced by the annihilations or decays of the DM particles. The collider detection is to detect the DM particles produced at high energy colliders. It is essential to combine all the experimental results and achieve a complete picture of DM.

4.3 Direct detection

The direct detection is to detect the nuclear recoil signatures induced by the scattering of DM particles off the target nuclei in underground detectors [55]. For the DM particle with a mass of $\sim O(10^2)$ GeV and a local velocity of $\sim 10^{-3}c$, the typical energy scale of the scattering is $O(10)$ keV. The expected differential event rate per nucleus is

$$\frac{\mathrm{d}R}{\mathrm{d}E_R} = \frac{\rho_\chi}{m_\chi}\int_{v_{\min}}^{v_{\max}} \mathrm{d}^3v\ f(\boldsymbol{v})v\frac{\mathrm{d}\sigma(\boldsymbol{v},E_R)}{\mathrm{d}E_R} \tag{32}$$

where E_R is the nuclear recoil energy, ρ_χ is the local DM mass density, $f(\boldsymbol{v})$ is the DM velocity distribution in the lab frame which can be derived from the DM velocity distribution in the Galaxy frame, $\mathrm{d}\sigma/\mathrm{d}E_R$ is the cross section of the scattering between DM particles and target nuclei. The DM velocity distribution in the Galaxy is usually assumed to be the Maxwell–Boltzmann distribution. The upper limit of the DM velocity is determined by the escape velocity of DM in the Galaxy v_{esc}, which is typically taken as 500–600 km·s^{-1}.

Different interactions between DM particles and nuclei require different experimental materials and technics. For the majorana DM fermions, there are two typical operators describing the interaction between the DM particles and quarks, namely, scalar interaction $\bar{\chi}\chi\bar{q}q$ and axial-vector interaction $\bar{\chi}\gamma^\mu\gamma^5\chi\bar{q}\gamma_\mu\gamma_5 q$ (see e.g. Ref. [50]). In the realistic DM models (e.g. SUSY model), these two interactions could be mediated by the Higgs and Z bosons, respectively. In the non-relativistic limit, the scalar interaction does not depend on the spin of the nucleon. The scattering cross section would be coherently enhanced by a factor of A^2, where A is the atom number of the nucleus. This means heavy nuclei are suitable to detect such spin-independent (SI) interaction. For the axial-vector interaction, the $\gamma_i\gamma_5$ components lead to a three dimension vector current which is proportional to the particle angular momentum. Therefore, this interaction is spin-dependent (SD). Compared with SI interaction, there is no coherent enhancement for SD interaction. Since the nucleus spin is contributed by the un-paired nucleon, only the nuclei with an odd number of nucleons, such as ^{19}F, ^{127}I and so on, can be used to search for SD interaction.

There are three kinds of signatures induced by nuclear recoil events, namely, scintillation, ionization, and phonons. Some experiments only search for one kind of signal, while some detectors can measure two kinds of signals which are helpful to reduce the backgrounds. The direct detection experiments should be located in deep underground to shield from the CR background. The main backgrounds are electronic recoil events induced by the gamma-rays and electrons emitted from the radioactive isotopes in the surrounding rocks, air and the detector apparatus. Therefore the good shielding and high purity of the materials are required for experiments.

Some collaborations, such as DAMA [56], CoGeNT [57] and CRESST-II [58], have reported anomalous events which may be produced by DM. The DAMA collaboration has detected a modulation signature with a very high confidence level in the 2–6 keV energy interval in a long time. This observation can be interpreted by the annual modulation of the DM-nucleus scattering due to the Earth rotation around the Sun, where the DM particle has a small mass of $\sim$ 10 GeV and a large SI scattering cross section of $\sim O(10^{-40})$ cm^2 [59, 60]. The results from CoGeNT and CRESST-II can be marginally consistent with the DAMA result in the light DM scenario. However, such results conflict with the null results from the other experiments, such as XENON [61, 62]. The experimental uncertainties [63] and astrophysical uncertainties [64, 65] are difficult to relax the tensions among different experiments. Many new exotic DM models have been proposed in the literature, such as inelastic scattering DM [66, 67] and isospin violation DM [64, 68]. However, there is still no consistent interpretation for all the observations.

As shown in Fig. 10, the most stringent constraint on SI DM-nucleon cross section is set by XENON, which is a dual phase noble liquid detector located in Gran Sasso [62]. Since the detector only observes the recoil signatures above a threshold energy, it is not sensitive to the light DM particles. For a DM particle with a mass of 55 GeV, the upper-limit reaches 2×10^{-45} cm^2. In the future, the sensitivity of XENON will be improved by a magnitude of two orders [77]. Note that the XENON results have excluded some preferred parameter regions of the CMSSM. In particular, the pure higgsino DM is

strongly disfavored due to the large SI interaction with nucleons.

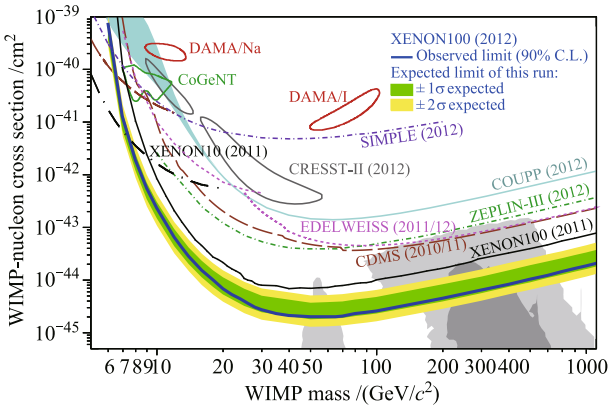

Fig. 10 Constraints on the SI DM-nucleon scattering cross section by XENON100. Also shown are results from DAMA [56, 59], CoGeNT [57], CRESST-II [58], CDMS [69, 70], EDELWEISS [71], SIMPLE [72], COUPP [82], ZEPLIN-III [73], and XENON10 [61], together with the preferred regions in CMSSM [74–76]. Reproduced from Ref. [62].

Figure 11 shows the recent limits on the SD DM-nucleon scattering cross section given by XENON100 [78] and other experiments. Since the nucleus spin is carried by the un-paired proton or neutron, different nuclei have different sensitivities for the SD DM-proton and DM-neutron interactions. The superheated liquid experiments containing ^{19}F, such as PICASSO [81], COUPP [82] and SIMPLE [72], set the most stringent constraints on the DM-proton scattering cross section[2]. The most strong limits on the DM-neutron cross section are given by XENON100.

4.4 Indirect detection

4.4.1 Antimatter particles

DM annihilations in the Galaxy would produce charged antimatter particles, such as positrons, anti-protons, and anti-deuterons. The charged particles interact with Galactic magnetic fields and the interstellar medium (ISM), and lose much information of the source. The propagation process can be described by the diffusion-loss equation (see e.g. Refs. [85–88])

$$\frac{\partial}{\partial t}\frac{\mathrm{d}n}{\mathrm{d}E} = \nabla\cdot\left[D(E,\boldsymbol{x})\nabla\frac{\mathrm{d}n}{\mathrm{d}E}\right] + \frac{\partial}{\partial t}\left[b(E,\boldsymbol{x})\frac{\mathrm{d}n}{\mathrm{d}E}\right] + Q(E,\boldsymbol{x},t) \quad (33)$$

where $\mathrm{d}n/\mathrm{d}E$ is the differential particle number density, D is the diffusion coefficient, b is the energy loss rate,

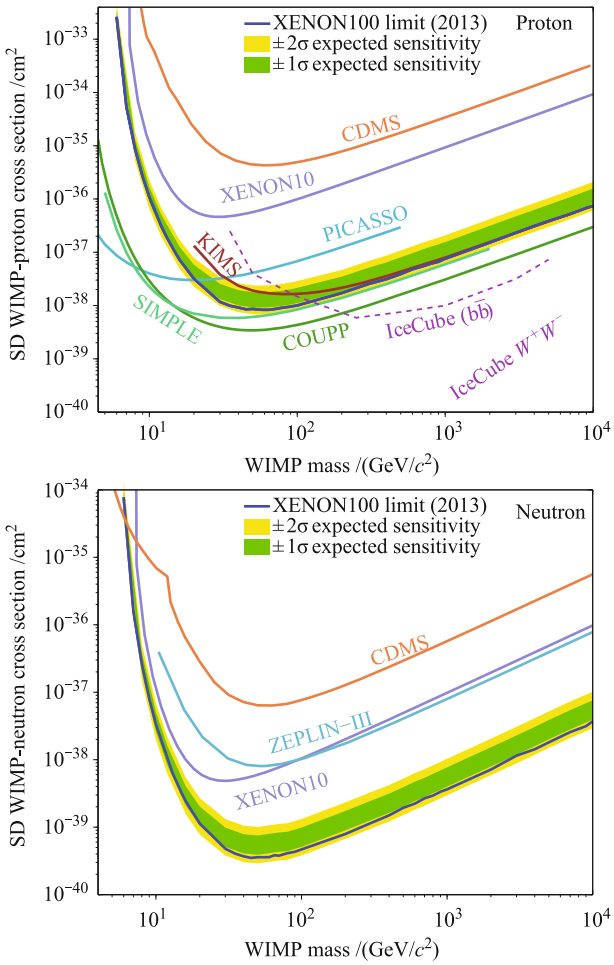

Fig. 11 Constraints on the SD scattering cross section for DM-proton (*top*) and DM-neutron (*bottom*) interactions given by XENON100. Also shown are results from XENON10 [79], CDMS [70, 80], ZEPLIN-III [73], PICASSO [81], COUPP [82], SIMPLE [72], KIMS [83], and IceCube [84]. Reproduced from Ref. [78].

and Q is the source term. In general, D and b are the functions of the energy and the position. The energy loss rate depends on the processes of inverse Compton scattering (ICS) and synchrotron radiation. The diffusion parameter $D = D_0E^{-\delta}$ could be determined by the CR observations, such as the ratios B/C and ^{10}Be/^{9}Be [102, 104–106].

The antimatter particles in the CR are produced by the p-p collisions between primary CR protons and ISM. Since the observed flux of CR protons is $\sim E^{-2.7}$, the flux of secondary positrons is expected to fall off quickly (e.g. $\sim E^{-2.7-\delta}$) at the high energy due to the diffusion [85–88]. However, the early HEAT [89, 90] and AMS-01 [91] measurements of the positron fraction $\phi(e^+)/(\phi(e^-)+\phi(e^+))$ have shown the hints of the excess positrons above $\sim$ 10 GeV. In 2008, the satellite

[2] As discussed in Section 4.4.3, the constraints from the neutrino detection depend on the branching fractions of particular DM annihilation channels into neutrinos.

based detector PAMELA confirmed such excess with high significance, as shown in the upper panel of Fig. 12 [92]. The solid curve is the expected fraction of secondary CR positrons. There is an obvious excess above 10 GeV which cannot be explained by the conventional CR model[3]. Recently, the space station based experiment AMS-02 released the new data of the positron fraction [93]. The AMS-02 detector has a larger aperture than PAMELA; it confirmed and improved the previous PAMELA result with a high significance.

The balloon based experiment ATIC reported the total flux of the CR electrons and positrons in 2008 [94]. As shown in the lower panel of Fig. 12, there is a sharp peak at $\sim$ 600 GeV, which also cannot be explained by the CR model. Fermi-LAT [95] and the ground-based Cerenkov telescope HESS [96, 97] also found an similar excess at the electron/positron spectrum. All these observations suggest the existence of some exotic high energy electron/positron sources.

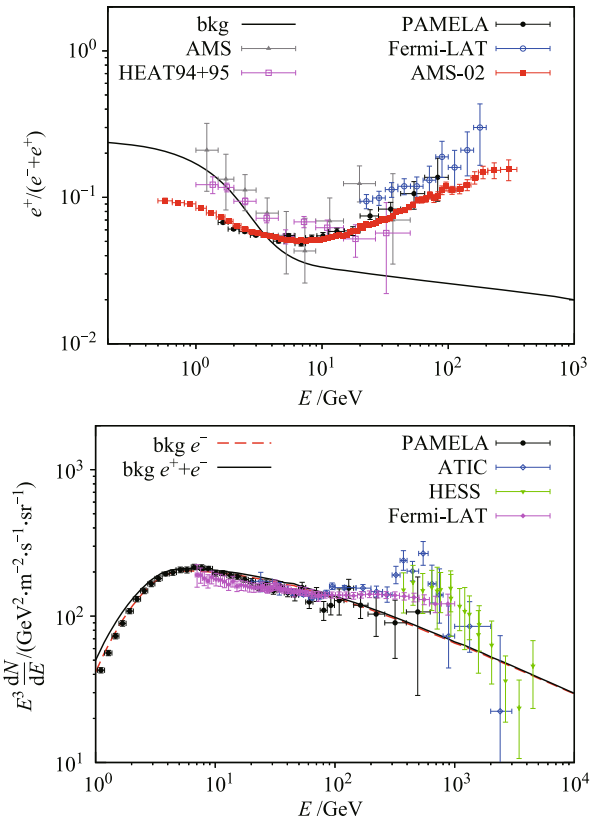

Fig. 12 Observational data of the positron fraction $\phi(e^+)/(\phi(e^-)+\phi(e^+))$ (*upper*) and the electron/positron flux (*lower*). Lines in these figures are the expectations based on conventional CR propagation models. Also shown are the experimental results from HEAT [89, 90], AMS-01 [91], PAMELA [92], Fermi [98], and AMS-02 [93] for the positron fraction, and ATIC [94], Fermi [95], HESS [96, 97], and PAMELA [99] for the electron/positron flux.

If the electron/positron excesses are induced by DM, it requires the DM particles have some exotic features. Since the observation of antiproton-to-proton ratio by PAMELA is consistent with the CR model [100], this means the DM particles dominantly interact with leptons rather than quarks and gauge bosons. Another important issue is that the production rate of the anomalous electrons/positrons should be very large. For the annihilating DM, it requires a large boost factor of $O(10^2) \sim O(10^3)$, which is defined as the ratio of the required DM annihilation cross section to the "natural value" 3×10^{-26} cm^3·s^{-1} (see e.g. Refs. [101, 104–106]).

Many models have been proposed in the literature to interpret this large boost factor, such as nearby DM substructures [107], non-thermal DM production [108], Breit–Wigner enhancement [109–111] and Sommerfeld enhancement [101, 112, 113]. In the sommerfeld enhancement scenario, the DM annihilation cross section is significantly enhanced by the long range attractive force at low velocities mediated by a new light boson ϕ; the annihilation process is assumed to be $\chi\chi \to \phi\phi \to f\bar{f}f\bar{f}$. Moreover, if the new boson is lighter than $\sim$ 1 GeV, the production of antiprotons is kinematically forbidden. Another attractive scenario is the "decaying DM", in which the DM particles would decay very slowly to SM particles [114–118]. To explain the experimental data, the lifetime of DM should be $\sim O(10^{26})$ s. Such long lifetime can be easily obtained by some high energy scale suppressed operators.

Finally, it should be noted that the anomalous electrons/positrons can be also interpreted by the astrophysical sources, such as pulsars and pulsar wind nebulae [119–125]. Unlike the continuously distributed and time independent DM source, astrophysical sources are discrete and time dependent. It is possible to distinguish these scenarios by future observations.

4.4.2 Photons

Unlike charged particles, detecting photons and neutrinos could resolve the information of the DM source since their directions and energy spectra are less affected during the propagation. The photons and neutrinos produced by far sources might also be observed, while only the charged particles produced by nearby sources within $\sim$ 1 kpc could be detected.

The fluxes of photons and neutrinos observed at the earth are given by (see e.g. Ref. [126])

[3] Since the influence of the solar wind on the positrons with energy below $\sim$ 10 GeV is unclear, the theoretic curve at the low energy may be not consistent with the experimental data.

$$\left(\frac{\mathrm{d}N}{\mathrm{d}E}\right)^A = \frac{1}{4\pi}\frac{\langle\sigma v\rangle}{2m_\chi^2}\left(\frac{\mathrm{d}N}{\mathrm{d}E}\right)_i^A \times J^A(\Delta\Omega) \quad (34)$$

$$\left(\frac{\mathrm{d}N}{\mathrm{d}E}\right)^D = \frac{1}{4\pi}\frac{1}{\tau_\chi m_\chi}\left(\frac{\mathrm{d}N}{\mathrm{d}E}\right)_i^D \times J^D(\Delta\Omega) \quad (35)$$

where the superscripts A and D denote annihilating and decaying DM respectively, τ_χ is the lifetime of decaying DM, $(\mathrm{d}N/\mathrm{d}E)_i$ is the initial energy spectrum. The J-factor J^A and J^D are defined as the line-of-sight (l.o.s.) integrals of the DM density ρ toward a direction of observation ψ integrated over a solid angle $\Delta\Omega$:

$$J^A(\Delta\Omega) = \int \mathrm{d}\Omega \int_{\mathrm{l.o.s.}} \mathrm{d}l \;\; \rho^2[r(l,\psi)] \quad (36)$$

$$J^D(\Delta\Omega) = \int \mathrm{d}\Omega \int_{\mathrm{l.o.s.}} \mathrm{d}l \;\; \rho[r(l,\psi)] \quad (37)$$

Here ρ is the DM density distribution which can be determined by N-body simulations. A commonly used form of ρ for the halo is given by

$$\rho(r) = \frac{\rho_0}{(r/R)^\gamma[1+(r/R)^\alpha]^{(\beta-\gamma)/\alpha}} \quad (38)$$

where $\rho_0 \sim 0.4$ GeV·cm^{-3} is the DM density in the Solar system. If the parameter set is taken to be $\alpha = 1$, $\beta = 3$ and $\gamma = 1$, Eq. (38) describes the Navarro–Frenk–White (NFW) profile [127].

The initial spectra depend on the detailed DM model. In general, the photons would be produced by the cascade decay or the final state radiation of the DM annihilation/decay products. The DM induced high energy electrons and positrons can also generate photons via the ICS, synchrotron radiation and bremsstrahlung radiation processes. These DM induced photons might cover from radio band to gamma-ray band. Here we focus on the detection of high energy gamma-ray photons. The satellite Fermi-LAT is one of the most important detector for gamma-rays. It can observe the high energy photons up to ~ 300 GeV. The ground-based atmospheric Cerenkov telescopes, such as HESS, VERITAS and MAGIC, can cover higher energy region, and are suitable for detecting heavy DM.

The DM dense regions are ideal targets to search for the DM signatures, such as dwarf galaxies [128–132], galaxy clusters [133–138], the Galactic halo [139–142] and the Galactic Center (GC) [143–147]. The dwarf galaxies are DM dominated objects, and do not have large gas components. Therefore, the dwarf galaxies are background free targets for the DM induced gamma-rays. The Fermi-LAT collaboration do not found any gamma-ray signature from the target dwarf galaxies from the first 11-month data, and set limits on the DM annihilation cross section [128]. Figure 13 shows the 95% confidence level upper limits on the DM annihilation cross section. It can be seen that for the light DM with a mass $\lesssim 30$ GeV and final states of $b\bar{b}$ and $\tau^+\tau^-$, the "natural value" of DM annihilation cross section 3×10^{-26} cm^3·s^{-1} has been excluded by the Fermi-LAT results.

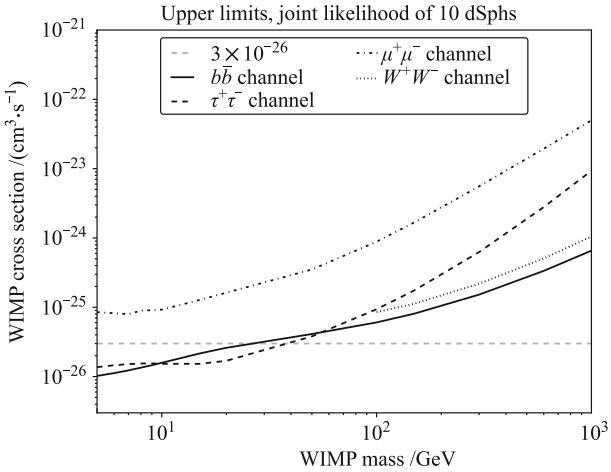

Fig. 13 Fermi 95% confidence level upper limits on the WIMP annihilation cross section for the channels of $b\bar{b}$, W^+W^-, $\mu^+\mu^-$, and $\tau^+\tau^-$. Reproduced from Ref. [128].

The J-factor of the GC is much larger than those of dwarf galaxies and galaxy clusters due to its short distance from the Earth and the large DM density. In general, the DM annihilation signatures from the GC should be strongest. However, the DM density in the inner GC is still unclear. Moreover, since the astrophysical gamma-ray backgrounds in the GC are very complicated, it is difficult to identify the DM signatures. Some studies claimed that a gamma-ray excess is found in the GC by using Fermi data [148, 149]. Such excess can be interpreted by the annihilation of DM particles with a mass of $\sim O(10)$ GeV.

The DM particles may annihilate into a pair of photons or a photon plus a Z or Higgs boson which result a gamma-ray line signature with the energy of m_χ or $m_\chi(1-m_{Z,h}^2/4m_\chi^2)$ [150–153]. Such signature is considered as the "smoking-gun" diagnostic for the existence of DM. Since the line emissions is usually induced by the loop process, the flux is expected to be much smaller than the continuous emissions. In 2012, some groups reported a possible line feature around 130 GeV from the GC in Fermi data with a significance larger than 3σ [154–158]. The origin of the possible line feature at the gamma-ray spectrum is still under debate. If this feature is the DM annihilation signature, it requires the DM particle with a mass of ~ 130 GeV and an annihilation cross section of $\sim 10^{-27}$ cm^3·s^{-1}, which is much larger than the ordinary predictions. In the latest analysis, the Fermi collaboration reported that no globally significant spec-

tral line signals are confirmed, and only a feature at 133 GeV with a global significance of 1.6σ was found [159]. The experiments with high energy resolutions, such as AMS-02, CALET and DAMPE, will be helpful to test this feature in the future.

4.4.3 Neutrinos

There are two kinds of DM induced neutrino signatures, namely solar neutrinos and cosmic neutrinos. First we discuss the former one. DM particles would be gradationally attracted by the Sun and lose energies by collisions with nuclei [160, 161]. If DM particles are trapped in the center of the Sun, they may have large annihilation rate due to large number density [162]. When the capture and annihilation processes reach equilibrium over a long time scale, the DM annihilation rate is determined by the capture rate. Note that the DM capture rate is proportional to the DM-nucleon scattering cross section [163, 164]. Unlike the other indirect detections, such solar neutrino detection would determine the DM-nucleon scattering cross section rather than the annihilation cross section.

The DM annihilation channels of e^+e^- and $\mu^+\mu^-$ do not contribute to neutrino signatures. If the products of DM annihilations are $\tau^+\tau^-$, W^+W^-, ZZ and $t\bar{t}$, they produce energetic neutrinos via cascade decays. For the annihilation channels into quarks, since neutrinos are generated from hadron decays after hadronization processes, the neutrino spectra are soft.

Once produced in the solar center, the high energy neutrinos interact with the matter before they escape from the Sun. The propagation of neutrinos are under the influences of neutral current interaction, charged current interaction, and tau neutrino regeneration process [165–167]. The other important propagation effects include the MSW matter effect in the Sun and the vacuum oscillations during the propogation.

Since the neutrino only has weak interactions with the matter, it can only be observed indirectly through the charged leptons generated by neutrinos interacting with the nuclei inside or near the detector. When the secondary high energy electrons and muons travel through the detector, the emitted Cerenkov radiation can be observed. The energy and direction information of neutrinos will be reconstructed by Cerenkov emissions. To improve the detection efficiency, the neutrino telescopes, such as Super-Kamiokande (Super-K), ANTARES and IceCube, usually have very large volumes.

Since the high energy atmospheric muons can travel a long distance in the matter, neutrino telescopes are set in the deep underground, water or ice, and usually only observe the up-going neutrinos to reduce the atmospheric muon background. The irreducible background is the up-going neutrinos produced by the CRs interacting with nuclei in the atmosphere [168]. The atmospheric neutrino backgrounds are almost isotropic, while the DM induced neutrinos are generated from particular directions. Furthermore, the atmospheric neutrino spectrum decreases as $\sim E^{-3.7}$, while the DM induced neutrino spectrum may be hard at energies near the mass of DM particles. Therefore, high angular and energy resolutions are essential to search the neutrino signature.

Recently, the IceCube collaboration reported the result of high energy solar neutrinos with the 79-string configuration [84]. No DM induced neutrino event has been found. The IceCube collaboration set upper limits on the DM-proton scattering cross section for two typical annihilation channels of $b\bar{b}$ ("soft") and W^+W^- ("hard"). For the SI interaction, the limits from IceCube are weaker than the CDMS and XENON. As shown in the top panel of Fig. 11, if the branching fraction of the DM annihilation channel into W^+W^- is 100%, IceCube gives the most strong constraints for the DM particles with masses larger than ~ 30 GeV.

Finally we briefly discuss the comic neutrinos from DM. The flux of cosmic neutrinos from DM is similar to the photons discussed in Section 4.4.2. The GC is the best region to search for the DM induced cosmic neutrino signature [169–173, 175]. Compared with the photon detection, the astrophysical background for the cosmic neutrino detection is also free. By using the outer volume as a veto and the central DeepCore strings with dense module density [174], IceCube has the capability to detect the down-going neutrinos from the GC. The limits on the DM annihilation cross section for $m_\chi \sim 1$ TeV are $10^{-23}\text{cm}^3\cdot\text{s}^{-1}$ and $10^{-22}\text{cm}^3\cdot\text{s}^{-1}$ for the $\nu\bar{\nu}$ and W^+W^- channels, respectively [175].

4.5 Collider detection

Since the WIMP mass is $\sim O(10^2)$ GeV, it is expected to produce these particles at high energy colliders, such as Tevatron, LHC and ILC. Since WIMPs almost do not interact with the matter, they will escape from the detector quickly without energy deposition and cannot be observed directly. Due to the momentum conservation in the plane perpendicular to the beam pipe, a crucial variable for the collider DM detection, called as "missing transverse energy" (MET), can be constructed by the associated products, such as jets, photons and leptons. The measurement of MET may determine the mass and the other important properties of the DM particle [176–181].

If the DM particles are directly produced by the

collisions of initial beams, an energetic jet or photon from the initial state radiation is required to trigger the signature. Such signals are called as "mono-jet" or "mono-photon", and are essential at hadron colliders and electron-positron colliders, respectively.

The collisions of initial beams may directly produce some heavy BSM particles (e.g. gluinos and squarks in the SUSY model). These particles would decay into DM particles via long decay chains. The final states depend on the mass spectra and the detailed interactions of the BSM particles. In such cases, the signatures are usually classified by the multiplicity of jets, b jets and leptons [182, 183].

One kind of background arises from QCD multi-jets since the energy measurement and the reconstruction of jets have some uncertainties. The limited detector coverage, the presence of dead regions and the noises may also contribute to "fake MET". The large MET cut condition, e.g. $\not{E}^T > 100$ GeV, would be helpful to reduce these backgrounds. The dominant SM backgrounds MET are the neutrinos generated by $Z(\to \nu\bar{\nu})$+jets, $W(\to l\nu)$+jets, $t\bar{t}$ and single top production. Many kinematic variables, such as razor [184, 185], α_T [186, 187] and M_{T2} [188–190], have been proposed to extract the signatures from the backgrounds.

Figure 14 shows the constraints on the DM-nucleon scattering cross section given by the ATLAS mono-jet research, compared with the results from direct detections [191]. In this analysis, four typical effective DM-quark interaction operators and one DM-gluon interaction operator are taken into account [192] (see also Refs. [195–200]). Since light DM particles are easily produced due to the phase space and the parton distribution function, the collider has strong capability to detect light DM particles with masses smaller than ~ 10 GeV. The sensitivities of direct detections for such light DM are limited due to the experimental thresholds. Another advantage of the collider detection is the comparable sensitivities for SI and SD interactions since both the scalar and axial-vector operators have similar behaviors in the relativistic limit at colliders. It can be seen from Fig. 14 that the ATLAS constraint on the SD scattering cross section $\sim O(10^{-40})\mathrm{cm}^2$ are more stringent than those given by direct detections.

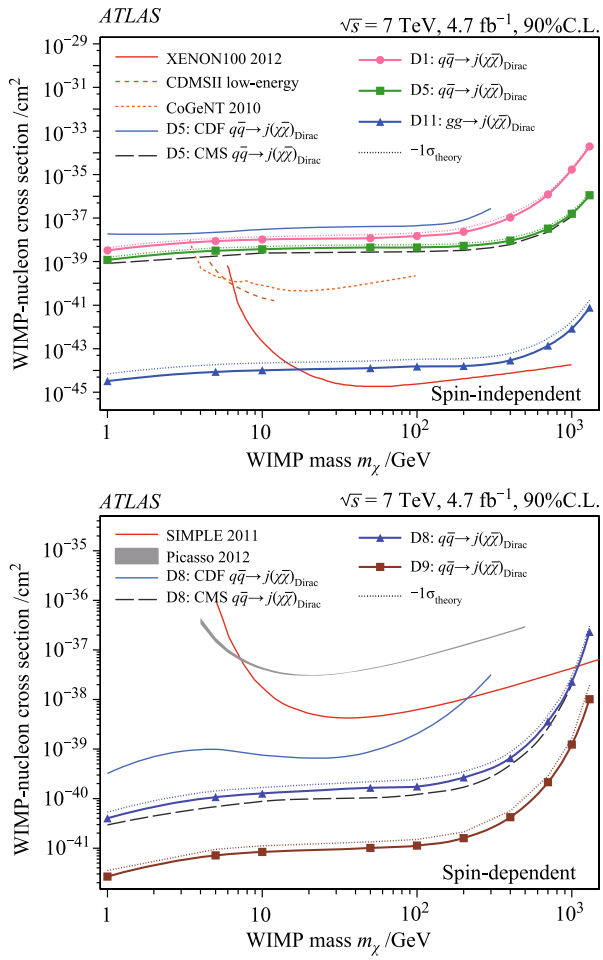

Fig. 14 Inferred ATLAS 90% limits on SI (*top*) and SD (*bottom*) DM-nucleon scattering cross sections. D1, D5, D8, D9 and D11 denote the effective interaction operators $\bar{\chi}\chi\bar{q}q$ (scalar), $\bar{\chi}\gamma^\mu\chi\bar{q}\gamma_\mu q$ (vector), $\bar{\chi}\gamma^\mu\gamma^5\chi\bar{q}\gamma_\mu\gamma_5 q$ (axial-vector), $\bar{\chi}\sigma^{\mu\nu}\chi\bar{q}\sigma_{\mu\nu}q$ (tensor) and $\bar{\chi}\chi(G^a_{\mu\nu})^2$ (scalar), respectively [192]. Also shown are the limits from XENON100 [62], CDMS [70], CoGeNT [57], SIMPLE [72], PICASSO [81], CDF [193], and CMS [194]. Reproduced from Ref. [191].

5 Big bang nucleosynthesis and lithium puzzle

5.1 Lithium puzzle

Big Bang cosmology is an excellent model to describe our Universe [201], which is based on two assumptions: Einstein's general relativity and cosmological Copernican principle. Here Copernican principle means that the Universe is homogeneous and isotropic on large scale. From the picture of the model, the Cosmos began from a dense and hot singularity (called "Big Bang") and has been expanding and cooling for about 13.7 billion years [202]. The model is supported by observational evidences such as Hubble's law, cosmic microwave background radiation and primordial element abundances, especially helium-4.

If the Cosmic is hot enough, a kind of particles can gain enough energy and turn to another; when the temperature goes down, such processes are suppressed and some particles never interact with others, so we call the particles "decouple". Two important decoupling processes

are usually mentioned in literature: light nuclei forming ("Big Bang Nucleosynthesis", or BBN) and photons decoupling from electrons (then form cosmic microwave background radiation, or CMB).

BBN happens from about a minute to about an hour after "Big Bang", and forms hydrogen-2 (or deuteron), helium-3, helium-4 (α-particle), lithium-7 and lithium-6. Heavier nuclei are formed little because of too short time interval. Primordial α-particle abundance can be easily estimated from proton-neutron ratio, and the result matches observation very well, so BBN is counted as a building block of Big Bang cosmology model. Detailed calculation procedure of these primordial element abundances has been set up since 1967 [203]. However, there is a "Lithium puzzle" – the calculation result of primordial lithium-7 abundance deviates from observation by a factor of ~ 3 [204], and observational lithium-6 is about 1000 times higher than theoretical prediction [205].

Extensive investigations have focused on the lithium puzzle. The discrepancy could be due to astrophysical or nuclear origin. Most literature consider pictures different from above (above picture can be denoted as "Standard" BBN, or SBBN), including varying the nucleon effective couplings and mass parameters, new particles/resonances (especially involving dark matter particles) in thermal nuclear reactions, and non-thermal electromagnetic or hadronic energy injection.

5.2 Cosmic rays during BBM as the origin of lithium puzzle

We also propose a non-thermal solution phenomenologically [206], by not going far from SBBN. In order to destroy lithium-7 and perhaps produce lithium-6, we have to include new contributions from non-thermal particles, which are dubbed as BBN cosmic rays (BBNCRs), and even the endothermic reactions. Our studies focus on budget and spectrum of the energy injected, and examine possible MeV-range nuclear reaction processes.

Possible candidate for BBNCR particles is hydrogens, namely protons, deuterons and tritones, whose intensity must be much lower than that of the corresponding SBBN particles. The ratio, denoted as ϵ, is taken to be small in order to keep the success of SBBN model. In order not to change deuterium abundance significantly, we must avoid non-thermal contributions from reaction $^7\mathrm{D} + p \to n + 2p$, whose threshold energy is 3.337 MeV. In order to destroy lithium-7, the most effective reaction is $^7\mathrm{Be} + p \to p + \alpha + {}^3\mathrm{He}$, whose threshold energy is 1.814 MeV. So BBNCRs play a role between the energy range from 1.814 MeV to 3.337 MeV. With lack of knowledge of the acceleration mechanism, we simply assume the BBNCR spectrum obeys a power law. The amount of BBNCRs is required to decrease quickly above 3.337 MeV. Below 1.814 MeV until the background SBBN particles, we choose a power law distribution with a lower index to lower the total energy budget. Besides $^7\mathrm{Be} + p \to p + \alpha + {}^3\mathrm{He}$, another important reactions to destroy lithium-7 is $^7\mathrm{Li} + p \to n + {}^7\mathrm{Be}$, and there are also reactions to renew lithium-7, e.g. $^3\mathrm{He} + \alpha \to \gamma + {}^7\mathrm{Be}$[4].

If we assume $\epsilon = 7 \times 10^{-5}$, 70% lithium-7 can be destroyed, and the discrepancy between theoretical prediction and observations can be filled. However, lithium-6 can only be lifted an order of magnitude, still less than observations.

In order to solve the Lithium puzzle, a lot of works are needed. Even for the single BBNCRs proposal, there are still more works, for examples

cross section measurements for several nuclear reactions, especially cross section for $^7\mathrm{Be} + p \to p + \alpha + {}^3\mathrm{He}$ is critical.

acceleration mechanism for BBNCRs, and such studies may be related with dark matter.

discriminant of BBNCRs, namely with how high accuracy in observation to make this mechanism apart from other solutions.

6 Discussion and conclusions

We briefly described our understanding on the current researches on Higgs physics, top quark, dark matter and lithium puzzle respectively. No confirmed BSM signals have been found! Currently LHC are running, and the high intensity Super-B factory will take data in the near future. The planned future colliders, like the Higgs Factories, are under intensive discussions. At the same time, lots of non-accelerator experiments are running or under construction. The crucial question is still there: Where is the BSM?

Acknowledgements This research was supported in part by the National Natural Science Foundation of China under grant numbers 11075003, 10821504, 11075194, 11105157, and 11135003, and the Postdoctoral Science Foundation of China under grant numbers 2012M510564 and 2012M520098.

References and notes

1. S. H. Zhu, Recent progress in physics beyond the standard model, *Front. Phys.*, 2013, 8(3): 241

[4] Relic primordial lithium-7 mainly (about 90%) comes from the decay of beryllium-7.

2. G. Aad, et al. [ATLAS Collaboration], Observation of a new particle in the search for the Standard Model Higgs boson with the ATLAS detector at the LHC, *Phys. Lett. B*, 2012, 716: 1, arXiv: 1207.7214
3. S. Chatrchyan, et al. [CMS Collaboration], Observation of a new boson at a mass of 125 GeV with the CMS experiment at the LHC, *Phys. Lett. B*, 2012, 716: 30, 1207.7235
4. T. Li, X. Wan, Y.-K. Wang, and S.-H. Zhu, Constraints on the universal varying Yukawa couplings: from SM-like to fermiophobic, *J. High Energy Phys.*, 2012, 1209: 086, arXiv: 1203.5083 [hep-ph]
5. S. H. Zhu, Complex vacuum and lightness of Higgs boson, arXiv: 1211.2370 [hep-ph], 2012
6. A. Sakharov, Quark-muonic currents and violation of CP invariance, *Pisma Zh. Eksp. Teor. Fiz.*, 1967, 5: 32
7. A. Riotto and M. Trodden, Recent progress in baryogenesis, *Ann. Rev. Nucl. Part. Sci.*, 1999, 49: 35, arXiv: hep-ph/9901362
8. T. Lee, A theory of spontaneous T violation, *Phys. Rev. D*, 1973, 8(4): 1226
9. T. Lee, CP nonconservation and spontaneous symmetry breaking, *Phys. Rep.*, 1974, 9(2): 143
10. C. Huang and S. H. Zhu, Erratum: $B \to X_s\tau^+\tau^-$ in a CP spontaneously broken two Higgs doublet model, *Phys. Rev. D*, 2000, 61(1): 015011, arXiv: hep-ph/9905463
11. C. S. Huang, W. Liao, Q. S. Yan, and S. H. Zhu, Rare decay $B \to X_s l^+ l^-$ in a CP spontaneously broken two Higgs doublet model, *Eur. Phys. J. C*, 2002, 25(1): 103, arXiv: hep-ph/0110147
12. S. Weinberg, Gauge theory of CP nonconservation, *Phys. Rev. Lett.*, 1976, 37(11): 657
13. G. C. Branco, Spontaneous CP nonconservation and natural flavor conservation: A minimal model, *Phys. Rev. D*, 1980, 22(11): 2901
14. K. Shizuya and S. Tye, Higgs-particle mixing and CP violation, *Phys. Rev. D*, 1981, 23(7): 1613
15. S. Zhu, Complete next-to-leading order QCD corrections to charged Higgs boson associated production with top quark at the CERN large hadron collider, *Phys. Rev. D*, 2003, 67(7): 075006, arXiv: hep-ph/0112109
16. Q.-H. Cao, X.Wan, X.-P.Wang and S.-H. Zhu, Searching for charged Higgs boson in polarized top quark, *Phys. Rev. D*, 2013, 87: 055022, arXiv:1301.6608 [hep-ph]
17. T. Aaltonen, et al. [CDF Collaboration], Measurement of the top quark forward-backward production asymmetry and its dependence on event kinematic properties, *Phys. Rev. D*, 2013, 87: 092002, arXiv: 1211.1003
18. V. M. Abazov, et al. [D0 Collaboration], Measurement of leptonic asymmetries and top quark polarization in $t\bar{t}$ production, arXiv: 1207.0364, 2012
19. T. Aaltonen, et al. [CDF Collaboration], Angular cross section for $t\bar{t}$ production, *Conf. Note*, 2013: 10974
20. G. Aad, et al. [ATLAS Collaboration], ATLAS measurement of the top quark pair production charge asymmetry in proton-proton collisions at $\sqrt{s} = 7$ TeV using the ATLAS detector, ATLAS-CONF-2013-078
21. S. Chatrchyan, et al. [CMS Collaboration], Inclusive and differential measurements of the $t\bar{t}$ charge asymmetry in proton-proton collisions at $\sqrt{s} = 7$ TeV, *Phys. Lett. B*, 2012, 717: 129, arXiv: 1207.0065 [hep-ex]
22. J. H. Kuhn and G. Rodrigo, Charge asymmetry of heavy quarks at hadron colliders, *Phys. Rev. D*, 1999, 59(5): 054017, arXiv: hep-ph/9807420
23. W. Bernreuther and Z. G. Si, Distributions and correlations for top quark pair production and decay at the Tevatron and LHC, *Nucl. Phys. B*, 2010, 837(1–2): 90, arXiv: 1003.392
24. V. Ahrens, A. Ferroglia, M. Neubert, B. D. Pecjak, and L. L. Yang, The top-pair forward-backward asymmetry beyond NLO, *Phys. Rev. D*, 2011, 84(7): 074004, arXiv: 1106.6051
25. M. Czakon, P. Fiedler, A. Mitov, and J. Rojo, Further exploration of top pair hadroproduction at NNLO, arXiv: 1305.3892, 2013
26. S. Jung, H. Murayama, A. Pierce, and J. D. Wells, Top quark forward-backward asymmetry from new t-channel physics, *Phys. Rev. D*, 2010, 81(1): 015004, arXiv: 0907.4112
27. K. Cheung, W. Y. Keung, and T. C. Yuan, Top quark forward-backward asymmetry, *Phys. Lett. B*, 2009, 682(3): 287, 0908.258
28. P. H. Frampton, J. Shu, and K. Wang, Axigluon as possible explanation for $p\bar{p} \to t\bar{t}$ forward-backward asymmetry, *Phys. Lett. B*, 2010, 683(4–5): 294, arXiv: 0911.295
29. J. Shu, K. Wang, and G. Zhu, A revisit to top quark forward-backward asymmetry, *Phys. Rev. D*, 2012, 85: 034008, arXiv: 1104.0083
30. B. Xiao, Y. Wang, and S. Zhu, Forward-backward asymmetry and differential cross section of top quark in flavor violating Z' model at $\mathcal{O}(\alpha_s^2\alpha_X)$, *Phys. Rev. D*, 2010, 82(3): 034026, arXiv: 1006.2510
31. S. Chatrchyan, et al. [CMS Collaboration], Search for same-sign top-quark pair production at $\sqrt{s}$ =7 TeV and limits on flavour changing neutral currents in the top sector, *J. High Energy Phys.*, 2011, 1108: 005, arXiv: 1106.2142
32. B. Xiao, Y. K. Wang, Z. Q. Zhou, and S. Zhu, Edge charge asymmetry in top pair production at the LHC, *Phys. Rev. D*, 2011, 83(5): 057503, arXiv: 1101.250
33. H. Wang, Y. Wang, B. Xiao, and S.-H. Zhu, New color-octet axial vector boson revisited, *Phys. Rev. D*, 2011, 84(9): 094019, 1107.576
34. T. Li, X. Wan, Y. K. Wang, and S.-H. Zhu, Distinguishing the color octet axial-vector-like particle for top quark asymmetry via color flow method at the LHC, arXiv: 1306.3586, 2013
35. J. Gallicchio and M. D. Schwartz, Seeing in color: Jet superstructure, *Phys. Rev. Lett.*, 2010, 105(2): 022001, arXiv: 1001.5027

36. F. Zwicky, Spectral displacement of extra galactic nebulae, *Helv. Phys. Acta*, 1933, 6: 110

37. H. W. Babcock, The rotation of the andromeda nebula, *Lick. Observatory. Bulletin*, 1939, 19: 41

38. V. C. Rubin, W. K. Jr. Ford, and N. Thonnard, Rotational properties of 21 SC galaxies with a large range of luminosities and radii, from NGC 4605 /R = 4kpc/to UGC 2885 /R = 122 kpc, *Astrophys. J.*, 1980, 238: 471

39. V. C. Rubin, D. Burstein, W. K. Jr. Ford, and N. Thonnard, Rotation velocities of 16 SA galaxies and a comparison of Sa, Sb, and SC rotation properties, *Astrophys. J.*, 1985, 289: 81

40. D. Clowe, M. Bradac, A. H. Gonzalez, M. Markevitch, S. W. Randall, C. Jones, and D. Zaritsky, A direct empirical proof of the existence of dark matter, *Astrophys. J.*, 2006, 648(2): L109, arXiv: astro-ph/0608407

41. G. Hinshaw, et al. [WMAP Collaboration], Nine-year wilkinson microwave anisotropy probe (WMAP) observations: Cosmological parameter results, arXiv: 1212.5226 [astro-ph.CO]

42. P. A. R. Ade, et al. [Planck Collaboration], Planck 2013 results. XVI. Cosmological parameters, arXiv: 1303.5076 [astro-ph.CO]

43. A. G. Riess, et al. [Supernova Search Team Collaboration], Observational evidence from supernovae for an accelerating universe and a cosmological constant, *Astron. J.*, 1998, 116(3): 1009, arXiv: astro-ph/9805201

44. S. Perlmutter, et al. [Supernova Cosmology Project Collaboration], Measurements of Omega and Lambda from 42 high redshift supernovae, *Astrophys. J.*, 1999, 517(2): 565, arXiv: astro-ph/9812133

45. B. A. Reid, W. J. Percival, D. J. Eisenstein, L. Verde, et al., Cosmological constraints from the clustering of the sloan digital sky survey DR7 luminous red galaxies, *Mon. Not. Roy. Astron. Soc.*, 2010, 404: 60, arXiv: 0907.1659 [astro-ph.CO]

46. B. A. Reid, L. Samushia, M. White, W. J. Percival, et al., The clustering of galaxies in the SDSS-III Baryon Oscillation Spectroscopic Survey: Measurements of the growth of structure and expansion rate at z=0.57 from anisotropic clustering, arXiv: 1203.6641 [astro-ph.CO], 2012

47. M. Taoso, G. Bertone, and A. Masiero, Dark matter candidates: A ten-point test, *J. cosmol. Astropart. Phys.*, 2008, 0803: 022, arXiv: 0711.4996 [astro-ph]

48. G. Bertone, D. Hooper, and J. Silk, Particle dark matter: Evidence, candidates and constraints, *Phys. Rep.*, 2005, 405(5–6): 279, arXiv: hep-ph/0404175

49. E. W. Kolb and M. S. Turner, The Early Universe, New York: Addison-Wesley, 1990

50. G. Jungman, M. Kamionkowski, and K. Griest, Supersymmetric dark matter, *Phys. Rep.*, 1996, 267(5–6): 195, arXiv: hep-ph/9506380

51. D. Hooper and S. Profumo, Dark matter and collider phenomenology of universal extra dimensions, *Phys. Rep.*, 2007, 453(2–4): 29, arXiv: hep-ph/0701197

52. S. Dodelson and L. M. Widrow, Sterile-neutrinos as dark matter, *Phys. Rev. Lett.*, 1994, 72(1): 17, arXiv: hep-ph/9303287

53. X. D. Shi and G. M. Fuller, A New dark matter candidate: Nonthermal sterile neutrinos, *Phys. Rev. Lett.*, 1999, 82(14): 2832, arXiv: astro-ph/9810076

54. S. J. Asztalos, L. J. Rosenberg, K. van Bibber, P. Sikivie, and K. Zioutas, Searches for astrophysical and cosmological axions, *Ann. Rev. Nucl. Part. Sci.*, 2006, 56(1): 293

55. M. W. Goodman and E. Witten, Detectability of certain dark matter candidates, *Phys. Rev. D*, 1985, 31(12): 3059

56. R. Bernabei, et al. [DAMA Collaboration], First results from DAMA/LIBRA and the combined results with DAMA/NaI, *Eur. Phys. J. C*, 2008, 56: 333, arXiv: 0804.2741 [astro-ph]

57. C. E. Aalseth, et al. [CoGeNT Collaboration], Results from a search for light-mass dark matter with a P-type point contact germanium detector, *Phys. Rev. Lett.*, 2011, 106: 131301, arXiv: 1002.4703 [astro-ph.CO]

58. G. Angloher, M. Bauer, I. Bavykina, A. Bento, et al., Results from 730 kg days of the CRESST-II dark matter search, *Eur. Phys. J. C*, 2012, 72: 1971, arXiv: 1109.0702 [astro-ph.CO]

59. C. Savage, G. Gelmini, P. Gondolo, and K. Freese, Compatibility of DAMA/LIBRA dark matter detection with other searches, *J. Cosmol. Astropart. Phys.*, 2009, 0904: 010, arXiv: 0808.3607 [astro-ph]

60. S. Chang, A. Pierce, and N. Weiner, Using the energy spectrum at DAMA/LIBRA to probe light dark matter, *Phys. Rev. D*, 2009, 79: 115011, arXiv: 0808.0196 [hep-ph]

61. J. Angle, et al. [XENON10 Collaboration], A search for light dark matter in XENON10 data, *Phys. Rev. Lett.*, 2011,107: 051301, arXiv: 1104.3088 [astro-ph.CO]

62. E. Aprile, et al. [XENON100 Collaboration], Dark matter results from 225 live days of XENON100 data, *Phys. Rev. Lett.*, 2012, 109: 181301, arXiv: 1207.5988 [astro-ph.CO]

63. D. Hooper, J. I. Collar, J. Hall, D. McKinsey, and C. Kelso, A consistent dark matter interpretation for CoGeNT and DAMA/LIBRA, *Phys. Rev. D*, 2010, 82: 123509, arXiv: 1007.1005 [hep-ph]

64. P. J. Fox, J. Liu, and N. Weiner, Integrating out astrophysical uncertainties, *Phys. Rev. D*, 2011, 83: 103514, arXiv: 1011.1915 [hep-ph]

65. T. Schwetz, Direct detection data and possible hints for low-mass WIMPs, *PoS IDM*, 2011, 2010: 070, arXiv: 1011.5432 [hep-ph]

66. D. Tucker-Smith and N. Weiner, Inelastic dark matter, *Phys. Rev. D*, 2001, 64(4): 043502, arXiv: hep-ph/0101138

67. S. Chang, G. D. Kribs, D. Tucker-Smith, and N. Weiner, Inelastic dark matter in light of DAMA/LIBRA, *Phys. Rev. D*, 2009, 79: 043513, arXiv: 0807.2250 [hep-ph]

68. J. L. Feng, J. Kumar, D. Marfatia, and D. Sanford, Isospin-violating dark matter, *Phys. Lett. B*, 2011, 703: 124, arXiv: 1102.4331 [hep-ph]

69. Z. Ahmed, et al. [CDMS-II Collaboration], Dark matter search results from the CDMS II experiment, *Science*, 2010, 327: 1619, arXiv: 0912.3592 [astro-ph.CO]
70. Z. Ahmed, et al. [CDMS-II Collaboration], Results from a low-energy analysis of the CDMS II germanium data, *Phys. Rev. Lett.*, 2011, 106: 131302, arXiv: 1011.2482 [astro-ph.CO]
71. E. Armengaud, et al. [EDELWEISS Collaboration], Final results of the EDELWEISS-II WIMP search using a 4-kg array of cryogenic germanium detectors with interleaved electrodes, *Phys. Lett. B*, 2011, 702: 329, arXiv: 1103.4070 [astro-ph.CO]
72. M. Felizardo, T. A. Girard, T. Morlat, A. C. Fernandes, et al., Final analysis and results of the phase II SIMPLE dark matter search, *Phys. Rev. Lett.*, 2012, 108: 201302, arXiv: 1106.3014 [astro-ph.CO]
73. D. Y. Akimov, H. M. Araujo, E. J. Barnes, V. A. Belov, et al., WIMP-nucleon cross-section results from the second science run of ZEPLIN-III, *Phys. Lett. B*, 2012, 709: 14, arXiv: 1110.4769 [astro-ph.CO]
74. O. Buchmueller, et al., Higgs and supersymmetry, *Eur. Phys. J. C*, 2012, 72: 2020, arXiv: 1112.3564 [hep-ph]
75. C. Strege, et al., Updated global fits of the cMSSM including the latest LHC SUSY and Higgs searches and XENON100 data, *J. Cosmol. Astropart. Phys.*, 2012, 1203: 030, arXiv: 1112.4192 [hep-ph]
76. A. Fowlie, et al., The CMSSM favoring new territories: The impact of new LHC limits and a 125 GeV Higgs, *Phys. Rev. D*, 2012, 86: 075010, arXiv:1206.0264 [hep-ph]
77. E. Aprile [XENON1T Collaboration], The XENON1T dark matter search experiment, arXiv: 1206.6288 [astro-ph.IM], 2012
78. E. Aprile, et al. [XENON100 Collaboration], Limits on spin-dependent WIMP-nucleon cross sections from 225 live days of XENON100 data, arXiv: 1301.6620 [astroph.CO], 2013
79. J. Angle, E. Aprile, F. Arneodo, L. Baudis, et al., Limits on spin-dependent WIMP-nucleon crosssections from the XENON10 experiment, *Phys. Rev. Lett.*, 2008, 101: 091301, arXiv: 0805.2939 [astro-ph]
80. Z. Ahmed, et al. [CDMS Collaboration], Search for weakly interacting massive particles with the first five-tower data from the cryogenic dark matter search at the Soudan underground laboratory, *Phys. Rev. Lett.*, 2009, 102: 011301, arXiv: 0802.3530 [astro-ph]
81. S. Archambault, et al. [PICASSO Collaboration], Constraints on low-mass WIMP interactions on ^{19}F from PICASSO, *Phys. Lett. B*, 2012, 711: 153, arXiv: 1202.1240 [hep-ex]
82. E. Behnke, et al. [COUPP Collaboration], First dark matter search results from a 4-kg CF3I bubble chamber operated in a deep underground site, *Phys. Rev. D*, 2012, 86: 052001, arXiv: 1204.3094 [astro-ph.CO]
83. S. C. Kim, H. Bhang, J. H. Choi, W. G. Kang, et al., New limits on interactions between weakly interacting massive particles and nucleons obtained with CsI(Tl) crystal detectors, *Phys. Rev. Lett.*, 2012, 108: 181301, arXiv: 1204.2646 [astro-ph.CO]
84. M. G. Aartsen, et al. [IceCube Collaboration], Search for dark matter annihilations in the Sun with the 79-string IceCube detector, *Phys. Rev. Lett.*, 2013, 110: 131302, arXiv: 1212.4097 [astro-ph.HE]
85. E. A. Baltz and J. Edsjo, Positron propagation and fluxes from neutralino annihilation in the halo, *Phys. Rev. D*, 1998, 59(2): 023511, arXiv: astro-ph/9808243
86. I. V. Moskalenko and A. W. Strong, Production and propagation of cosmic ray positrons and electrons, *Astrophys. J.*, 1998, 493(2): 694, arXiv: astro-ph/9710124
87. I. V. Moskalenko and A. W. Strong, Positrons from particle dark-matter annihilation in the galactic halo: propagation green's functions, *Phys. Rev. D*, 1999, 60(6): 063003, arXiv: astro-ph/9905283
88. A. W. Strong, I. V. Moskalenko, and V. S. Ptuskin, Cosmic-ray propagation and interactions in the Galaxy, *Ann. Rev. Nucl. Part. Sci.*, 2007, 57(1): 285, arXiv: astro-ph/0701517
89. S. W. Barwick, et al. [HEAT Collaboration], Measurements of the cosmic ray positron fraction from 1 GeV to 50 GeV, *Astrophys. J.*, 1997, 482: L191, arXiv: astro-ph/9703192
90. S. Coutu, et al., Positron measurements with the HEAT-$\bar{p}$ instrument, in: International Cosmic Ray Conference (2001), Vol. 5 of International Cosmic Ray Conference, p. 1687
91. M. Aguilar, et al. [AMS-01 Collaboration], Cosmic-ray positron fraction measurement from 1 GeV to 30 GeV with AMS-01, *Phys. Lett. B*, 2007, 646: 145, arXiv: astro-ph/0703154 [astro-ph]
92. O. Adriani, et al. [PAMELA Collaboration], An anomalous positron abundance in cosmic rays with energies 1.5–100 GeV, *Nature*, 2009, 458: 607, arXiv: 0810.4995 [astro-ph]
93. M. Aguilar, et al. [AMS Collaboration], First result from the alpha magnetic spectrometer on the international space station: Precision measurement of the positron fraction in primary cosmic rays of 0.5–350 GeV, *Phys. Rev. Lett.*, 2013, 110(14): 141102
94. J. Chang, J. H. Adams, H. S. Ahn, G. L. Bashindzhagyan, M. Christl, O. Ganel, T. G. Guzik, J. Isbert, K. C. Kim, E. N. Kuznetsov, M. I. Panasyuk, A. D. Panov, W. K. H. Schmidt, E. S. Seo, N. V. Sokolskaya, J. W. Watts, J. P. Wefel, J. Wu, and V. I. Zatsepin, An excess of cosmic ray electrons at energies of 300–800 GeV, *Nature*, 2008, 456(7220): 362
95. M. Ackermann, et al. [Fermi LAT Collaboration], Fermi LAT observations of cosmic-ray electrons from 7 GeV to 1 TeV, *Phys. Rev. D*, 2010, 82: 092004, 1008.3999 [astro-ph.HE]
96. F. Aharonian, et al. [HESS Collaboration], The energy spectrum of cosmic-ray electrons at TeV energies, *Phys. Rev. Lett.*, 2008, 101: 261104, arXiv: 0811.3894 [astro-ph]
97. F. Aharonian, et al. [HESS Collaboration], Probing the ATIC peak in the cosmic-ray electron spectrum with HESS,

Astron. Astrophys., 2009, 508: 561, arXiv: 0905.0105 [astro-ph.HE]

98. M. Ackermann, et al. [Fermi LAT Collaboration], Measurement of separate cosmic-ray electron and positron spectra with the Fermi large area telescope, *Phys. Rev. Lett.*, 2012, 108: 011103, arXiv: 1109.0521 [astro-ph.HE]
99. O. Adriani, et al. [PAMELA Collaboration], The cosmic-ray electron flux measured by the PAMELA experiment between 1 and 625 GeV, *Phys. Rev. Lett.*, 2011, 106: 201101, arXiv: 1103.2880 [astro-ph.HE]
100. O. Adriani, G. C. Barbarino, G. A. Bazilevskaya, R. Bellotti, et al., A new measurement of the antiproton-to-proton flux ratio up to 100 GeV in the cosmic radiation, *Phys. Rev. Lett.*, 2009, 102: 051101, arXiv: 0810.4994 [astro-ph]
101. M. Cirelli, M. Kadastik, M. Raidal and A. Strumia, Model-independent implications of the e^+, e^-, anti-proton cosmic ray spectra on properties of Dark Matter, *Nucl. Phys. B*, 2009, 813: 1, arXiv: 0809.2409 [hep-ph]
102. T. Delahaye, R. Lineros, F. Donato, N. Fornengo and P. Salati, Positrons from dark matter annihilation in the galactic halo: Theoretical uncertainties, *Phys. Rev. D*, 2008, 77: 063527, arXiv: 0712.2312 [astro-ph]
103. T. Delahaye, F. Donato, N. Fornengo, J. Lavalle, R. Lineros, P. Salati and R. Taillet, Galactic secondary positron flux at the Earth, *Astron. Astrophys.*, 2009, 501: 821, arXiv: 0809.5268 [astro-ph]
104. J. Liu, Q. Yuan, X. J. Bi, H. Li and X. Zhang, A Markov chain Monte Carlo study on dark matter property related to the cosmic $e^{\pm}$ excesses, *Phys. Rev. D*, 2010, 81: 023516, arXiv: 0906.3858 [astro-ph.CO]
105. J. Liu, Q. Yuan, X. J. Bi, H. Li, and X. Zhang, Cos-RayMC: A global fitting method in studying the properties of the new sources of cosmic $e^{\pm}$ excesses, *Phys. Rev. D*, 2012, 85: 043507, arXiv: 1106.3882 [astro-ph.CO]
106. Q. Yuan, X. J. Bi, G. M. Chen, Y.Q. Guo, S. J. Lin, and X. Zhang, Implications of the AMS-02 positron fraction in cosmic rays, arXiv: 1304.1482 [astro-ph.HE], 2013
107. D. Hooper, A. Stebbins, and K. M. Zurek, Excesses in cosmic ray positron and electron spectra from a nearby clump of neutralino dark matter, *Phys. Rev. D*, 2009, 79: 103513, arXiv: 0812.3202 [hep-ph]
108. X.-J. Bi, R. Brandenberger, P. Gondolo, T.-J. Li, Q. Yuan, and X.-M. Zhang, Non-thermal production of WIMPs, cosmic $e^{\pm}$ excesses and gamma-rays from the galactic center, *Phys. Rev. D*, 2009, 80: 103502, arXiv: 0905.1253 [hep-ph]
109. D. Feldman, Z. Liu, and P. Nath, PAMELA positron excess as a signal from the hidden sector, *Phys. Rev. D*, 2009, 79: 063509, arXiv: 0810.5762 [hep-ph]
110. M. Ibe, H. Murayama, and T. T. Yanagida, Breit-Wigner enhancement of dark matter annihilation, *Phys. Rev. D*, 2009, 79: 095009: arXiv: 0812.0072 [hep-ph]
111. W.-L. Guo and Y.-L. Wu, Enhancement of dark matter annihilation via Breit–Wigner resonance, *Phys. Rev. D*, 2009, 79: 055012, arXiv: 0901.1450 [hep-ph]
112. M. Pospelov and A. Ritz, Astrophysical signatures of secluded dark matter, *Phys. Lett. B*, 2009, 671: 391, arXiv: 0810.1502 [hep-ph]
113. N. Arkani-Hamed, D. P. Finkbeiner, T. R. Slatyer, and N. Weiner, A theory of dark matter, *Phys. Rev. D*, 2009, 79: 015014, arXiv: 0810.0713 [hep-ph]
114. P.-F. Yin, Q. Yuan, J. Liu, J. Zhang, X.-J. Bi, S.-H. Zhu, and X.-M. Zhang, PAMELA data and leptonically decaying dark matter, *Phys. Rev. D*, 2009, 79: 023512, arXiv: 0811.0176 [hep-ph]
115. K. Ishiwata, S. Matsumoto, and T. Moroi, Cosmic-ray positron from superparticle dark matter and the PAMELA anomaly, *Phys. Lett. B*, 2009, 675: 446, arXiv: 0811.0250 [hep-ph]
116. A. Ibarra and D. Tran, Decaying dark matter and the PAMELA anomaly, *J. Cosmol. Astropart. Phys.*, 2009, 0902: 021, arXiv: 0811.1555 [hep-ph]
117. C.-R. Chen, M. M. Nojiri, F. Takahashi, and T. T. Yanagida, Decaying hidden gauge boson and the PAMELA and ATIC/PPB-BETS anomalies, *Prog. Theor. Phys.*, 2009, 122: 553, arXiv: 0811.3357 [astro-ph]
118. A. Arvanitaki, S. Dimopoulos, S. Dubovsky, P. W. Graham, R. Harnik, and S. Rajendran, Astrophysical probes of unification, *Phys. Rev. D*, 2009, 79: 105022, arXiv: 0812.2075 [hep-ph]
119. D. Hooper, P. Blasi, and P. D. Serpico, Pulsars as the sources of high energy cosmic ray positrons, *J. Cosmol. Astropart. Phys.*, 2009, 0901: 025, arXiv: 0810.1527 [astro-ph]
120. H. Yuksel, M. D. Kistler, and T. Stanev, TeV gamma rays from geminga and the origin of the GeV positron excess, *Phys. Rev. Lett.*, 2009, 103: 051101, arXiv: 0810.2784 [astro-ph]
121. S. Profumo, Dissecting cosmic-ray electron–positron data with Occam's Razor: The role of known Pulsars, *Central Eur. J. Phys.*, 2011, 10: 1, arXiv: 0812.4457 [astro-ph]
122. D. Malyshev, I. Cholis, and J. Gelfand, Pulsars versus dark matter interpretation of ATIC/PAMELA, *Phys. Rev. D*, 2009, 80: 063005, arXiv: 0903.1310 [astro-ph.HE]
123. T. Linden and S. Profumo, Probing the pulsar origin of the anomalous positron fraction with AMS-02 and atmospheric cherenkov telescopes, arXiv: 1304.1791 [astro-ph.HE], 2013
124. I. Cholis and D. Hooper, Dark matter and pulsar origins of the rising cosmic ray positron fraction in light of new data from AMS, arXiv: 1304.1840 [astro-ph.HE], 2013
125. P. F. Yin, Z. H. Yu, Q. Yuan, and X. J. Bi, Pulsar interpretation for the AMS-02 result, arXiv: 1304.4128 [astro-ph.HE], 2013
126. L. Bergstrom, P. Ullio, and J. H. Buckley, Observability of gamma-rays from dark matter neutralino annihilations in the Milky Way halo, *Astropart. Phys.*, 1998, 9(2): 137, arXiv: astro-ph/9712318
127. J. F. Navarro, C. S. Frenk, and S. D. M. White, The Structure of cold dark matter halos, *Astrophys. J.*, 1996, 462: 563, arXiv: astro-ph/9508025

128. M. Ackermann, et al. [Fermi-LAT Collaboration], Constraining dark matter models from a combined analysis of milky way satellites with the Fermi large area telescope, *Phys. Rev. Lett.*, 2011, 107: 241302, arXiv: 1108.3546 [astro-ph.HE]

129. A. Geringer-Sameth and S. M. Koushiappas, Exclusion of canonical WIMPs by the joint analysis of Milky Way dwarfs with Fermi, *Phys. Rev. Lett.*, 2011, 107: 241303, arXiv: 1108.2914 [astro-ph.CO]

130. I. Cholis and P. Salucci, Extracting limits on Dark Matter annihilation from gamma-ray observations towards dwarf spheroidal galaxies, *Phys. Rev. D*, 2012, 86: 023528, arXiv: 1203.2954 [astro-ph.HE]

131. M. N. Mazziotta, F. Loparco, F. de Palma, and N. Giglietto, A model independent analysis of the Fermi Large Area Telescope gamma-ray data from the Milky Way dwarf galaxies and halo to constrain dark matter scenarios, arXiv: 1203.6731 [astro-ph.IM], 2012

132. Y.-L. S. Tsai, Q. Yuan, and X. Huang, A generic method to constrain the dark matter model parameters from Fermi observations of dwarf spheroids, *J. Cosmol. Astropart. Phys.*, 2013, 1303: 018, arXiv: 1212.3990 [astro-ph.HE]

133. M. Ackermann, et al. [Fermi-LAT Collaboration], GeV gamma-ray flux upper limits from clusters of galaxies, arXiv: 1006.0748 [astro-ph.HE], 2010

134. Q. Yuan, P.-F. Yin, X.-J. Bi, X.-M. Zhang, and S.-H. Zhu, Gamma rays and neutrinos from dark matter annihilation in galaxy clusters, *Phys. Rev. D*, 2010, 82: 023506, arXiv: 1002.0197 [astro-ph.HE]

135. L. Dugger, T. E. Jeltema, and S. Profumo, Constraints on decaying dark matter from fermi observations of nearby galaxies and clusters, *J. Cosmol. Astropart. Phys.*, 2010, 1012: 015, arXiv: 1009.5988 [astro-ph.HE]

136. S. Ando and D. Nagai, Fermi-LAT constraints on dark matter annihilation cross section from observations of the Fornax cluster, *J. Cosmol. Astropart. Phys.*, 2012, 1207: 017, arXiv: 1201.0753 [astro-ph.HE]

137. J. Ke, M. Luo, L. Wang, and G. Zhu, Gamma-rays from nearby clusters: Constraints on selected decaying dark matter models, *Phys. Lett. B*, 2011, 698: 44, arXiv: 1101.5878 [hep-ph]

138. X. Huang, G. Vertongen, and C. Weniger, Probing dark matter decay and annihilation with Fermi LAT observations of nearby galaxy clusters, *J. Cosmol. Astropart. Phys.*, 2012, 1201: 042, arXiv: 1110.1529 [hep-ph]

139. M. Ackermann, et al. [LAT Collaboration], Constraints on the galactic Halo dark matter from Fermi-LAT diffuse measurements, *Astrophys. J.*, 2012, 761: 91, arXiv: 1205.6474 [astro-ph.CO]

140. J. Zhang, Q. Yuan, and X.-J. Bi, Galactic diffuse gamma rays — recalculation based on the new measurements of cosmic electron spectrum, *Astrophys. J.*, 2010, 720: 9, arXiv: 0908.1236 [astro-ph.HE]

141. M. Papucci and A. Strumia, Robust implications on Dark Matter from the first FERMI sky gamma map, *J. Cosmol. Astropart. Phys.*, 2010, 1003: 014, arXiv: 0912.0742 [hep-ph]

142. L. Zhang, C. Weniger, L. Maccione, J. Redondo, and G. Sigl, Constraining decaying dark matter with Fermi LAT gamma-rays, *J. Cosmol. Astropart. Phys.*, 2010, 1006: 027, arXiv: 0912.4504[astro-ph.HE]

143. P. D. Serpico and D. Hooper, Gamma-rays from dark matter annihilation in the central region of the galaxy, *New J. Phys.*, 2009, 11: 105010, arXiv: 0902.2539 [hep-ph]

144. J. Ellis, K. A. Olive, and V. C. Spanos, Galactic-centre gamma rays in CMSSM dark matter scenarios, *J. Cosmol. Astropart. Phys.*, 2011,1110: 024, arXiv: 1106.0768 [hep-ph]

145. T. Cohen, M. Lisanti, T. R. Slatyer, and J. G. Wacker, Illuminating the 130 GeV gamma line with continuum photons, *J. High Energy Phys.*, 2012, 1210: 134, arXiv: 1207.0800 [hep-ph]

146. I. Cholis, M. Tavakoli, and P. Ullio, Searching for the continuum spectrum photons correlated to the 130 GeV gamma-ray line, *Phys. Rev. D*, 2012, 86(8): 083525, arXiv: 1207.1468 [hep-ph]

147. X.-Y. Huang, Q. Yuan, P.-F. Yin, X.-J. Bi, and X.-L. Chen, Constraints on the dark matter annihilation scenario of Fermi 130 GeV γ-ray line emission by continuous gamma-rays, MilkyWay halo, galaxy clusters and dwarf galaxies observations, *J. Cosmol. Astropart. Phys.*, 2012, 1211: 048, arXiv: 1208.0267 [astro-ph.HE]

148. D. Hooper and L. Goodenough, Dark matter annihilation in the galactic center as seen by the Fermi gamma ray space telescope, *Phys. Lett. B*, 2011, 697: 412, arXiv: 1010.2752 [hep-ph]

149. D. Hooper and T. Linden, On the origin of the gamma rays from the galactic center, *Phys. Rev. D*, 2011, 84: 123005, arXiv: 1110.0006 [astro-ph.HE]

150. L. Bergstrom and H. Snellman, Observable monochromatic photons from cosmic photino annihilation, *Phys. Rev. D*, 1988, 37(12): 3737

151. S. Rudaz, On the annihilation of heavy neutral fermion pairs into monochromatic gamma-rays and its astrophysical implications, *Phys. Rev. D*, 1989, 39(12): 3549

152. L. Bergstrom and P. Ullio, Full one loop calculation of neutralino annihilation into two photons, *Nucl. Phys. B*, 1997, 504(1–2): 27, arXiv: hep-ph/9706232

153. P. Ullio and L. Bergstrom, Neutralino annihilation into a photon and a Z boson, *Phys. Rev. D*, 1998, 57(3): 1962, arXiv: hep-ph/9707333

154. T. Bringmann, X. Huang, A. Ibarra, S. Vogl, and C. Weniger, Fermi LAT search for internal Bremsstrahlung signatures from dark matter annihilation, *J. Cosmol. Astropart. Phys.*, 2012, 1207: 054, arXiv: 1203.1312 [hep-ph]

155. C. Weniger, A tentative gamma-ray line from dark matter annihilation at the Fermi large area telescope, *J. Cosmol. Astropart. Phys.*, 2012,1208: 007, arXiv: 1204.2797 [hep-ph]

156. E. Tempel, A. Hektor, and M. Raidal, Fermi 130 GeV gamma-ray excess and dark matter annihilation in sub-haloes and in the Galactic centre, *J. Cosmol. Astropart. Phys.*, 2012, 1209: 032 [Addendum-ibid., 2012, 1211: A01], arXiv: 1205.1045 [hep-ph]

157. A. Boyarsky, D. Malyshev, and O. Ruchayskiy, Spectral and spatial variations of the diffuse gamma-ray background in the vicinity of the Galactic plane and possible nature of the feature at 130 GeV, arXiv: 1205.4700 [astro-ph.HE], 2012

158. M. Su and D. P. Finkbeiner, Strong evidence for gamma-ray line emission from the inner galaxy, arXiv: 1206.1616 [astro-ph.HE], 2012

159. Fermi-LAT Collaboration, Search for gamma-ray spectral lines with the Fermi large area telescope and dark matter implications, arXiv: 1305.5597 [astro-ph.HE], 2013

160. J. Faulkner and R. L. Gilliland, Weakly interacting, massive particles and the solar neutrino flux, *Astrophys. J.*, 1985, 299: 994

161. W. H. Press and D. N. Spergel, Capture by the sun of a galactic population of weakly interacting massive particles, *Astrophys. J.*, 1985, 296: 679

162. J. Silk, K. A. Olive, and M. Srednicki, The Photino, the Sun and high-energy neutrinos, *Phys. Rev. Lett.*, 1985, 55(2): 257

163. A. Gould, Resonant enhancements in WIMP capture by the Earth, *Astrophys. J.*, 1987, 321: 571

164. A. Gould, Cosmological density of WIMPs from solar and terrestrial annihilations, *Astrophys. J.*, 1992, 388: 338

165. M. Cirelli, N. Fornengo, T. Montaruli, I. A. Sokalski, A. Strumia, and F. Vissani, Spectra of neutrinos from dark matter annihilations, *Nucl. Phys. B*, 2005, 727(1–2): 99 [Erratum-ibid. B, 2008, 790: 338], arXiv: hep-ph/0506298)

166. M. Blennow, J. Edsjo, and T. Ohlsson, Neutrinos from WIMP annihilations using a full three-flavor Monte Carlo, *J. Cosmol. Astropart. Phys.*, 2008, 0801: 021, arXiv: 0709.3898 [hep-ph]

167. V. Barger, W. -Y. Keung, G. Shaughnessy, and A. Tregre, High energy neutrinos from neutralino annihilations in the Sun, *Phys. Rev. D*, 2007, 76: 095008, arXiv: 0708.1325 [hep-ph]

168. M. Honda, T. Kajita, K. Kasahara, S. Midorikawa, and T. Sanuki, Calculation of atmospheric neutrino flux using the interaction model calibrated with atmospheric muon data, *Phys. Rev. D*, 2007, 75(4): 043006, arXiv: astro-ph/0611418

169. H. Yuksel, S. Horiuchi, J. F. Beacom, and S. 'i. Ando, Neutrino constraints on the dark matter total annihilation cross section, *Phys. Rev. D*, 2007, 76: 123506, arXiv: 0707.0196 [astro-ph]

170. J. Liu, P.-F. Yin, and S.-H. Zhu, Prospects for detecting neutrino signals from annihilating/decaying dark matter to account for the PAMELA and ATIC results, *Phys. Rev. D*, 2009, 79: 063522, arXiv: 0812.0964 [astro-ph]

171. A. E. Erkoca, G. Gelmini, M. H. Reno, and I. Sarcevic, Muon fluxes and showers from dark matter annihilation in the galactic center, *Phys. Rev. D*, 2010, 81: 096007, arXiv: 1002.2220 [hep-ph]

172. L. Covi, M. Grefe, A. Ibarra, and D. Tran, Neutrino signals from dark matter decay, *J. Cosmol. Astropart. Phys.*, 2010, 1004: 017, arXiv: 0912.3521 [hep-ph]

173. A. E. Erkoca, G. Gelmini, M. H. Reno, and I. Sarcevic, Muon fluxes and showers from dark matter annihilation in the galactic center, *Phys. Rev. D*, 2010, 81: 096007, arXiv: 1002.2220 [hep-ph]

174. R. Abbasi, et al. [IceCube Collaboration], The design and performance of IceCube DeepCore, *Astropart. Phys.*, 2012, 35: 615, arXiv: 1109.6096 [astro-ph.IM]

175. R. Abbasi, et al. [IceCube Collaboration], Search for neutrinos from annihilating dark matter in the direction of the galactic center with the 40-string IceCube neutrino observatory, arXiv: 1210.3557 [hep-ex], 2012

176. H. -C. Cheng, J. F. Gunion, Z. Han, G. Marandella, and B. McElrath, Mass determination in SUSY-like events with missing energy, *J. High Energy Phys.*, 2007, 0712: 076, arXiv: 0707.0030 [hep-ph]

177. M. Burns, K. Kong, K. T. Matchev, and M. Park, Using subsystem M_{T2} for complete mass determinations in decay chains with missing energy at hadron colliders, *J. High Energy Phys.*, 2009, 0903: 143, arXiv: 0810.5576 [hep-ph]

178. A. J. Barr and C. G. Lester, A review of the mass measurement techniques proposed for the large hadron collider, *J. Phys. G*, 2010, 37: 123001, arXiv: 1004.2732 [hep-ph]

179. T. Han, I.-W. Kim, and J. Song, Kinematic cusps with two missing particles I: Antler decay topology, *Phys. Rev. D*, 2013, 87: 035003, 2012, arXiv: 1206.5633 [hep-ph]

180. K. A. Olive, Colliders and Cosmology, In: Karlsruhe 2007, SUSY 2007, 158–173, arXiv: 0709.3303 [hep-ph], 2007

181. H. Baer and X. Tata, Dark matter and the LHC, arXiv: 0805.1905 [hep-ph], 2008

182. H. Baer, X. Tata, and J. Woodside, Multi-lepton signals from supersymmetry at hadron super colliders, *Phys. Rev. D*, 1992, 45(1): 142

183. D. Feldman, Z. Liu, and P. Nath, Sparticles at the LHC, *J. High Energy Phys.*, 2008, 0804: 054, arXiv: 0802.4085 [hep-ph]

184. C. Rogan, Kinematical variables towards new dynamics at the LHC, arXiv: 1006.2727 [hep-ph], 2010

185. CMS Collaboration, Search for supersymmetry with the razor variables at CMS, CMS-PAS-SUS-12-005

186. L. Randall and D. Tucker-Smith, Dijet searches for supersymmetry at the LHC, *Phys. Rev. Lett.*, 2008, 101: 221803, arXiv: 0806.1049 [hep-ph]

187. S. Chatrchyan, et al. [CMS Collaboration], Search for supersymmetry in final states with missing transverse energy and 0, 1, 2, or at least 3 b-quark jets in 7 TeV pp collisions using the variable alphaT, *J. High Energy Phys.*, 2013, 1301: 077, arXiv: 1210.8115 [hep-ex]

188. C. G. Lester and D. J. Summers, Measuring masses of semi-invisibly decaying particles pair produced at hadron colliders, *Phys. Lett. B*, 1999, 463: 99, arXiv: hep-ph/9906349

189. A. Barr, C. Lester, and P. Stephens, m_{T2}: The Truth behind the glamour, *J. Phys. G*, 2003, 29: 2343, arXiv: hep-ph/0304226

190. S. Chatrchyan, et al. [CMS Collaboration], Search for supersymmetry in hadronic final states using MT2 in *pp* collisions at $\sqrt{s} = 7$ TeV, *J. High Energy Phys.*, 2012, 1210: 018, arXiv: 1207.1798 [hep-ex]

191. G. Aad, et al. [ATLAS Collaboration], Search for dark matter candidates and large extra dimensions in events with a jet and missing transverse momentum with the ATLAS detector, *J. High Energy Phys.*, 2013,1304: 075, arXiv: 1210.4491 [hep-ex]

192. J. Goodman, M. Ibe, A. Rajaraman, W. Shepherd, T. M. P. Tait, and H.-B. Yu, Constraints on dark matter from colliders, *Phys. Rev. D*, 2010, 82: 116010, arXiv: 1008.1783 [hep-ph]

193. T. Aaltonen, et al. [CDF Collaboration], A search for dark matter in events with one jet and missing transverse energy in $p\bar{p}$ collisions at $\sqrt{s} = 1.96$ TeV, *Phys. Rev. Lett.,* 2012, 108: 211804, arXiv: 1203.0742 [hep-ex]

194. S. Chatrchyan, et al. [CMS Collaboration], Search for dark matter and large extra dimensions in monojet events in pp collisions at $\sqrt{s} = 7$ TeV, *J. High Energy Phys.*, 2012, 1209: 094, arXiv: 1206.5663 [hep-ex]

195. Y. Bai, P. J. Fox, and R. Harnik, The tevatron at the frontier of dark matter direct detection, *J. High Energy Phys.*, 2010, 1012: 048, arXiv: 1005.3797 [hep-ph]

196. P. J. Fox, R. Harnik, J. Kopp, and Y. Tsai, Missing energy signatures of dark matter at the LHC, *Phys. Rev. D*, 2012, 85: 056011, arXiv: 1109.4398 [hep-ph]

197. Q. -H. Cao,C. -R. Chen, C. S. Li, and H. Zhang, Effective dark matter model: Relic density, CDMS II, Fermi LAT and LHC, *J. High Energy Phys.*, 2011, 1108: 018, arXiv: 0912.4511 [hep-ph]

198. M. Beltran, D. Hooper, E. W. Kolb, and Z. C. Krusberg, Deducing the nature of dark matter from direct and indirect detection experiments in the absence of collider signatures of new physics, *Phys. Rev. D*, 2009, 80: 043509, arXiv: 0808.3384 [hep-ph]

199. J.-M. Zheng, Z.-H. Yu, J.-W. Shao, X.-J. Bi, Z. Li, and H.-H. Zhang, Constraining the interaction strength between dark matter and visible matter: I. fermionic dark matter, *Nucl. Phys. B*, 2012, 854: 350, arXiv: 1012.2022[hep-ph]

200. Z.-H. Yu, J.-M. Zheng, X.-J. Bi, Z. Li, D.-X. Yao, and H.-H. Zhang, Constraining the interaction strength between dark matter and visible matter: II. scalar, vector and spin-3/2 dark matter, *Nucl. Phys. B*, 2012, 860: 115, arXiv: 1112.6052 [hep-ph]

201. C. E. Rolfs and W. S. Rodney, Cauldrons in the Cosmos: Nuclear Astrophysics, Chicago: University of Chicago Press, 1988

202. Planck Collaboration, Planck 2013 results. I. Overview of products and scientific results, *Astron. Astrophys.*, (submitted), arXiv:1303.5062

203. R. V. Wagoner, W. A. Fowler, and F. Hoyle, On the synthesis of elements at very high temperatures, *Astrophys. J.*, 1967, 148: 3

204. A. Coc, S. Goriely, Y. Xu, M. Saimpert, and E. Vangioni, Standard big bang nucleosynthesis up to CNO with an improved extended nuclear network, *Astrophys. J.*, 2012, 744(2): 158

205. F. Hammache, M. Heil, S. Typel, D. Galaviz, K. Sümmerer, A. Coc, F. Uhlig, F. Attallah, M. Caamano, D. Cortina, H. Geissel, M. Hellström, N. Iwasa, J. Kiener, P. Koczon, B. Kohlmeyer, P. Mohr, E. Schwab, K. Schwarz, F. Schümann, P. Senger, O. Sorlin, V. Tatischeff, J. P. Thibaud, E. Vangioni, A. Wagner, and W. Walus, High-energy break-up of 6Li as a tool to study the Big-Bang nucleosynthesis reaction 2H(alpha,gamma)6Li, *Phys. Rev. C*, 2010, 82(6): 065803, arXiv: 1011.6179

206. M.-M. Kang, Y. Hu, H.-B. Hu, and S.-H. Zhu, Cosmic rays during BBN as origin of lithium problem, *J. Cosmol. Astropart. Phys.*, 2012, 1205: 011, arXiv: 1110.0163 [astro-ph.CO]